Journal of Medicinal Chemistry

ARTICLE

pubs.acs.org/jmc

Highly Potent, Selective, and Orally Active Phosphodiesterase 10A Inhibitors†

Michael S. Malamas,*[,‡] Yike Ni,[‡] James Erdei,[‡] Hans Stange,[∥] Rudolf Schindler,[∥] Hans-Joachim Lankau,[∥] Christian Grunwald,[∥] Kristi Yi Fan,[‡,#] Kevin Parris,[‡] Barbara Langen,[∥] Ute Egerland,[∥] Thorsten Hage,[∥] Karen L. Marquis,[‡] Steve Grauer,[‡] Julie Brennan,[‡] Rachel Navarra,[‡] Radka Graf,[‡] Boyd L. Harrison,[‡] Albert Robichaud,[‡,⊥] Thomas Kronbach,[∥] Menelas N. Pangalos,[‡,∞] Norbert Hoefgen,[∥] and Nicholas J. Brandon[§]

[‡]Pfizer Neuroscience Princeton, 865 Ridge Road, Monmouth Junction, New Jersey 08852, United States

[§]Pfizer Neuroscience, Eastern Point Road, Groton Connecticut 06340, United States

[∥]Biocrea Therapies GmbH, Meissner Strasse 191, 01445 Radebeul, Germany

Supporting Information

ABSTRACT: The identification of highly potent and orally active phenylpyrazines for the inhibition of PDE10A is reported. The new analogues exhibit subnanomolar potency for PDE10A, demonstrate high selectivity against all other members of the PDE family, and show desired druglike properties. Employing structure-based drug design approaches, we methodically explored two key regions of the binding pocket of the PDE10A enzyme to alter the planarity of the parent compound **1** and optimize its affinity for PDE10A. Bulky substituents at the C9 position led to elimination of the mutagenicity of **1**, while a crucial hydrogen bond interaction with Glu716 markedly enhanced its potency and selectivity. A systematic assessment of the ADME and PK properties of the new analogues led to druglike development candidates. One of the more potent compounds, **96**, displayed an IC_{50} for PDE10A of 0.7 nM and was active in predictive antipsychotic animal models.

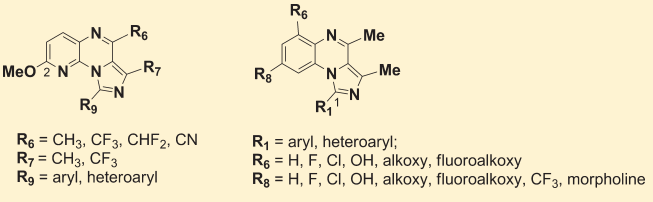

INTRODUCTION

Cyclic nucleotide phosphodiesterases (PDEs) are key regulators of cellular signal transduction by hydrolyzing the 3′,5′-monophosphate bond of the ubiquitous intracellular second messengers adenosine 3′,5′-monophosphate (cAMP) and cyclic guanosine 3′,5′-monophosphate (cGMP). Both cAMP and cGMP are important messengers in the signaling cascades of G-protein-coupled receptors, and modulation of their intracellular levels influences the magnitude and duration of cellular responses to hormonal and neurotransmitter stimulation. There are 11 distinct phosphodiesterases, designated as PDE1−PDE11. The PDEs are encoded by 21 different genes in humans, with over 50 isoforms expressed as a result of alternative splicing patterns.[1] PDEs are classified by their substrate specificity. Some selectively hydrolyze cAMP or cGMP, while others will accept both cyclic nucleotides as substrates.[2,3] The PDE families differ in the substrate specificity for the cyclic nucleotides, the mechanism of regulation, and the sensitivity to inhibitors. They are also localized to specific subcellular sites, which allows for fine spatial and temporal control of the levels of the cyclic nucleotides.[4,5] This feature is thought to be an important contributing factor that allows the enzyme to influence selective intracellular signaling pathways in response to different stimuli, in spite of the ubiquitous intracellular distribution of the cyclic nucleotides. PDE10A is a dual substrate PDE.[6−9] PDE10A hydrolyzes both cAMP and cGMP, with a higher affinity for cAMP (K_m = 0.05 μM) than for cGMP (K_m =3 μM).[10] PDE10A is primarily a membrane bound enzyme containing a catalytic domain in the C-terminal portion of the protein. Key residues of the catalytic core form a well-defined hydrophobic clamp region that positions the planar rings of the nucleotide for interaction with an absolutely conserved glutamine residue (Gln716 in PDE10A). Free rotation of this glutamine in PDE10A, and other dual substrate enzymes, is believed to allow the binding of either cAMP or cGMP in the substrate pocket.[11] PDE10A mRNA is highly expressed only in brain and testes.[7,8] In the brain, both PDE10A mRNA and protein are specifically enriched in the medium spiny neurons (MSNs) of the striatum.[12] PDE10A has been suggested to play a key role in regulating MSN activity and in turn striatal output, as this region integrates dopaminergic and glutamatergic inputs from midbrain and cortical regions, respectively, to action motoric and cognitive function. Dysfunction in cortical−striatal neurotransmission has been implicated in the pathophysiology of schizophrenia; thus, PDE10A inhibition has been suggested as a therapeutic strategy for this disease.[13−15]

Received: July 15, 2011
Published: October 11, 2011

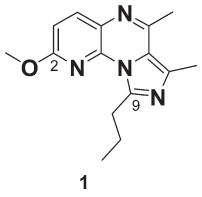

1

Figure 1

In a recent disclosure,[16] we have described the design of new pyrido[2,3-*e*]pyrazines (**1**, Figure 1) as potent and selective inhibitors of PDE10A. The reported research has resulted in the discovery of novel templates for PDE10A inhibition and has delineated key structural elements of the ligand and protein interactions. These initial structure−activity relationship (SAR) studies have paved the path to a better understanding of the requirements needed to enhance the ligand's potency and selectivity. X-ray crystallography and molecular modeling calculations were employed to assist with the design of new PDE10A inhibitors. The initial research effort has also encountered some shortcomings related to the pharmacokinetic properties and safety concerns because of the planar structure of the chemical scaffold that may hamper further development of these PDE10A inhibitors. In addition, we were aiming to further optimize the overall biology profile of the initial series, like target affinity and selectivity and in vitro potency. Armed with this information, we have employed a chemistry strategy to address these issues and further improve the pharmacokinetic and safety properties of our PDE10A inhibitors. Our key focus centered on the potential risk of mutagenicity of the early compounds. Activation of strain TA1537 (AMES test) should be indicative for ligand intercalation to DNA. Intercalation occurs when ligands of an appropriate size and chemical nature align between the base pairs of DNA. These ligands are mostly polycyclic, aromatic, and planar and therefore able to insert into the hydrophobic environment found between the base pairs. These structural modifications can lead to functional changes, often to the inhibition of transcription and replication and DNA repair processes, which make intercalators potent mutagens. The pyrido[2,3-*e*]pyrazine scaffold of our early inhibitors represents a fused polycyclic planar structure, which potentially intercalates with DNA. Initially, we have designed a new template to alter the three-dimensional structure of the parent compound **1**. Examination of the X-ray crystal structure of **1**:PDE10A[16] (Figure 2) revealed the presence of a large unoccupied region of the ligand binding pocket. We intended to take advantage of this observation and introduce bulky groups at the C9 position of the fused tricyclic ring system of the parent compound (Figure 1) in an attempt to alter the overall three-dimensional planarity of the parent compound. Such structural arrangement will break the three-dimensional planarity of the parent structure and prevent its intercalation with DNA. Furthermore, our chemistry strategy will focus on improving the metabolic stability and pharmacokinetic properties of the parent compound **1**. Isolation and characterization of the metabolites of **1** have indicated the areas of the molecule (2-OMe, 6- and 7-Me, 9-propyl), which were prone to metabolic oxidation (Figure 3). Masking of the metabolically labile alkyl functionalities of the parent compound **1** with more stable fluorine-containing groups will result in metabolic stability enhancement. In order to achieve these objectives in a timely manner, we have designed a unified chemistry methodology (Schemes 1−4). This new synthetic

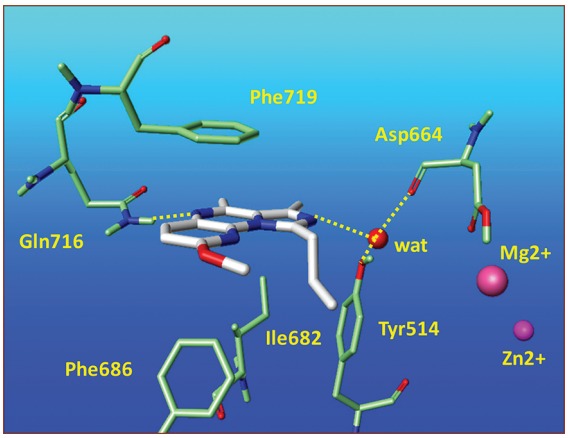

Figure 2. Crystal structure of PDE10A (rat) complexed with **1**,[16] highlighting the key hydrogen-bonding interactions between ligand and protein at the invariant Glu716, and the water-mediated contacts with Asp664 and Tyr514. The fused ring system of the ligand is sandwiched between residues Phe719, Ile682, and Phe686, making π-stacking interactions with Phe719, π-edge stacking with Phe686, and hydrophobic contact with Ile682.

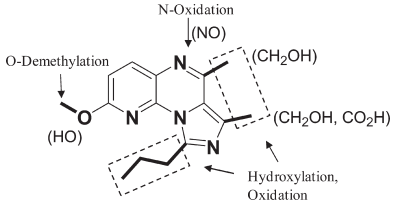

Figure 3. Metabolic disposition of **1** (shown are identified metabolites).

strategy enables us to introduce multiple group modifications on common synthetic blocks using parallel synthesis techniques. The scope of this paper will cover the advancements in safety, physicochemical properties, and pharmacokinetic properties of the parent compound **1**, as well as further improvements in ligand potency, selectivity, and in vivo efficacy.

CHEMISTRY

The compounds needed to delineate the SAR for this study were prepared according to synthetic Schemes 1−4. To expedite SAR development, we have designed a synthetic strategy to allow for parallel synthesis, enabling us to rapidly explore the C9 position of the parent template (compound **1**), as well as new scaffolds. An important process throughout the SAR studies was the preparation of bromoimidazole building blocks (i.e., **6**), which upon coupling with aryl groups, by employing the palladium-catalyzed cross-coupling Suzuki protocol, produced the target compounds. In Scheme 1, 2-chloropyridine **2** was treated with 4-methylimidazole in the presence of potassium hydroxide or potassium carbonate to afford the coupled product **3** in 4:1 isomeric ratio. Reduction of the nitro group of **3a** with Pd/C and ammonium formate produced aniline **3b**, which upon treatment with acetic anhydride in toluene furnished amide **4**. Cyclization of **4** to the tricyclic intermediate **5** was accomplished with phosphorus oxychloride and phosphorus pentoxide. Bromination of imidazole **5** with *N*-bromosuccinimide in acetonitrile produced bromoimidazole **6**, which was used for the preparation

dx.doi.org/10.1021/jm2009138 |*J. Med. Chem.* 2011, 54, 7621–7638

Scheme 1[a]

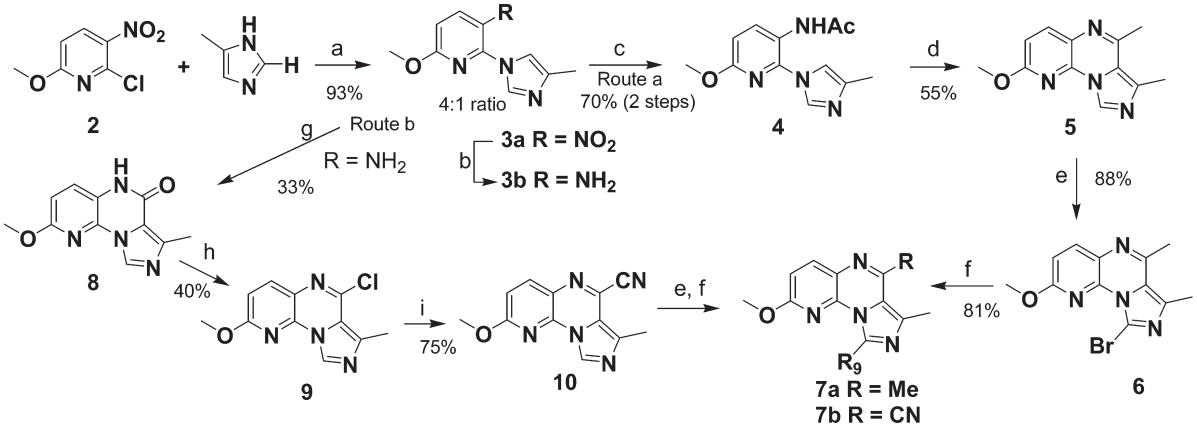

[a] Reagents: (a) KOH or K_2CO_3, DMF; (b) Pd/C, HCO_2NH_4, MeOH; (c) AC_2O, toluene; (d) P_2O5, $POCl_3$; e) *N*-bromosuccinimide, CH_3CN; (f) $R_9B(OH)_2$, K_2CO_3, $Pd(PPh_3)_4$, dioxane/H_2O, 3:1; (g) urea, CH_3CO_2H; (h) $POCl_3$; (i) Et_4NCN, DMSO.

Table 1. C9 Phenyl Substituted Analogues

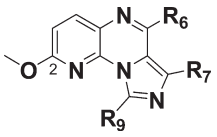

				IC$_{50}$ (nM)[a]		
compd	R_6	R_7	R_9	PDE10A	PDE2	microsomal stability, h/r, $t_{1/2}$ (min)[b]
1	Me	Me	CH_2CH_2Me	7.3 ± 0.6	270 ± 17.6	3/1
46	Me	Me	2-Me-Ph	7.4 ± 0.6	47 ± 7.5	18/3
47	Me	Me	2-CF_3-Ph	24 ± 3.2	135 ± 4.6	13/4
48	Me	Me	2-Cl-Ph	1.9 ± 0.2	11.6 ± 0.8	13/3
49	Me	Me	2,5-Cl,Cl-Ph	7.4 ± 0.7	11 ± 1.9	12/6
50	Me	Me	2,4-Cl,F-Ph	4.3 ± 0.4	27.5 ± 3.8	15/4
51	Me	Me	2-OMe-Ph	20.5 ± 1.3	64 ± 7.3	9/4
52	Me	Me	2-OCF_3-Ph	14.4 ± 0.8	237 ± 50.6	11/3
53	Me	Me	2-$CONH_2$-Ph	186 ± 14		>30/>30
54	Me	Me	3-$CONH_2$-Ph	1.8 ± 0.2	37 ± 4.6	>30/>30
55	Me	CF_3	2-Me-Ph	60 ± 17.9	19.5 ± 2.4	>30/13
56	Me	CF_3	2-Cl-Ph	44 ± 2.3	13.1 ± 0.8	27/22
57	Me	CF_3	2,5-Cl,Cl-Ph	173 ± 20.6	9.5 ± 0.5	>30/17
58	Me	CF_3	2,4-Cl,F-Ph	102 ± 6.4	29.9 ± 1.4	>30/24
59	Me	CF_3	2,5-Cl,F-Ph	87 ± 6.0	11.5 ± 0.5	>30/20
60	Me	CF_3	2,5-Cl,OMe-Ph	114 ± 11.5	7.4 ± 0.3	>30/3
61	CF_3	Me	2-Cl-Ph	197 ± 32.6	108 ± 12.5	>30/12
62	CHF_2	Me	2-Cl-Ph	7.3 ± 0.8	5.4 ± 0.7	24/8
63	CN	Me	2-Cl-Ph	6.0 ± 0.4	35.6 ± 3.5	16/4

[a] Mean of IC$_{50}$ with standard error of the mean; n = 4. [b] h = human. r = rat.

of synthetic libraries. Palladium-catalyzed cross-coupling reaction of **6** with any number of arylboronic and heteroarylboronic acids (Suzuki coupling[17]) in the presence of Pd(0) or Pd(II) catalyst under a variety of well-known conditions produced the desired products **7a** (entries **46**−**54**, **61**, and **62** (Table 1) and **64**−**80** (Table 2)). The cyano analogue **63** (Table 1) was prepared through an alternative synthetic route b. Imidazole **3b** was treated with urea to produce pyrazone **8**, which upon treatment with phosphorus oxychloride furnished choloropyrazine **9**. Displacement of the chlorine of pyrazine **9** with tetraethylammonium cyanide in dimethylsulfoxide afforded cyanopyrazine **10**. Compound **10** was converted to the desired final products **7b** as before. The trifluoromethyl-substituted analogues (**55**−**60**, Table 1) were prepared according to synthetic Scheme 2. Ethyl 2-chloro-4,4,4-trifluoroacetate **11** was treated with amidine to produce imidazole **12**. Coupling of **12** with 2-chloropyridine **13**

dx.doi.org/10.1021/jm2009138 |*J. Med. Chem.* 2011, 54, 7621–7638

Table 2. C9 Heteroaryl Substituted Analogues

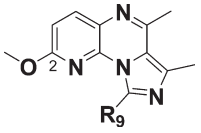

compd	R_9	IC_{50} (nM)[a] PDE10A	IC_{50} (nM)[a] PDE2	microsomal stability, h/r, $t_{1/2}$ (min)[b]
46	2-Me-Ph	7.4 ± 0.6	47 ± 7.5	18/3
64	2-(3-Me-thienyl)	2.8 ± 0.1	62 ± 6.5	6/2
65	2-(*N*-Me-pyrrole)	18.2 ± 1.0	276 ± 20.8	2/1
66	4-pyrazole	14.2 ± 1.6	299 ± 33.8	4/3
67	3,5-Me,Me-pyrazole	12.9 ± 1.1	27 ± 2.8	>30/>30
68	*N*-Me,3,5-Me,Me-pyrazole	6.1 ± 0.5	24.6 ± 1.9	>30/>30
69	3,5-Me,Me-isoxazole	46 ± 3.3		>30/12
70	2,4-Me,Me-thiazole	3.7 ± 0.3	30 ± 5.6	>30/9
71	5-pyrimidine	65.3 ± 5.0		27/25
72	3-pyridine	13.3 ± 1.4	32 ± 7.1	18/19
73	3-(2 Me-pyridine)	4.2 ± 0.4	17 ± 2.4	24/22
74	3-(4-Me-pyridine)	11 ± 1.1	38 ± 6.4	>30/25
75	3-(6-Me-pyridine)	73.4 ± 3.8		3/5
76	3-(4-Cl-pyridine)	7.9 ± 0.7	24 ± 2.3	15/6
77	4-(3-Me-pyridine)	5.2 ± 0.4	40.6 ± 6.0	>30/>30
78	4-(3-Cl-pyridine)	3.6 ± 0.3	18.4 ± 2.7	5/5
79	3-(2-MeO-pyridine)	13.9 ± 1,2	116 ± 15.6	>30/26
80	3-(4-MeO-pyridine)	14.9 ± 2.4	21.9 ± 1.7	>30/26

[a] Mean of IC_{50} with standard error of the mean; $n = 4$. [b] h = human. r = rat.

upon treatment with powdered KOH in *N*,*N*-dimethylformamide furnished imidazole **14**. Reduction of the nitro group of **14** to aniline with sodium bisulfate in acetic acid followed by in situ intramolecular cyclization of the aniline with the ester functionality furnished pyrazone **15**. Treatment of **15** with phosphorus oxychloride gave 2-chloropyrazine **16**, which upon treatment with trimethylaluminum in the presence of tetrakis(triphenylphosphine)palladium catalyst afforded pyrazine **17**. The intermediate **17** was converted to the desired products **18** (**55**−**60**, Table 1) as described in Scheme 1. The monosubstituted phenyl analogues (Table 3, entries **81**−**92**) were prepared from commercially available and appropriately substituted 2-fluoronitrobenzene in a similar manner as described above. The synthetic approaches depicted in Schemes 3 and 4 were utilized for the preparation of the highly functionalized phenylpyrazine derivatives contained in Table 3 (entries **93**−**122**). In Scheme 3, we have applied the same synthetic strategy as before by creating building blocks **32b** to increase the diversity and efficiency for the preparation of multiple analogues in this series. Building highly functionalized nitrophenyl intermediates **23**, **24**, **25b**, **26**, and **27** allowed the rapid generation of analogues to address several key SAR objectives related to ligand's potency, selectivity, and metabolic stability. The nitrophenyl analogues **23** and **24** were prepared from the corresponding substituted benzenes **19** and **20** upon treatment with nitric acid in dichloromethane. For the preparation of nitrophenyl **25b**, first, aniline **21a** was chlorinated at the ortho position with *N*-chlorosuccinimide and then was oxidized with sodium perborate. Application of the same oxidation protocol on aniline **21b** yielded compound **26**. The difluoromethoxy intermediate **27** was prepared from nitrophenol **22** upon alkylation with sodium chlorodifluoroacetate. During the execution of this work we were able to introduce the 2-bromo-4-methylimidazole at an earlier step and decrease the synthetic steps. In some instances, depending on the substitution of the nitrophenyl intermediate, the more reactive 4-methylimidazole was used in the displacement reaction as described in Scheme 1. Electron withdrawing groups on the nitrophenyl intermediate (i.e., **25b**) caused a slow coupling reaction and furnished low yields. Additional functionalization of the phenyl moiety of the imidazole adducts **28** and **28a** was achieved upon treatment with potassium methoxide in methanol to generate the methoxy analogues **29** and **30**. Imidazoles **28**−**30** were converted to the desired final products **33** as described before in Scheme 1. Modifications of the alkoxy groups at positions C6 and C8 were accomplished as shown in Scheme 4. Methoxy analogues **34** and **37** were treated with boron tribromide in dichloroethane to produce phenols **35** and **38a**. An alternative route was used for the preparation of phenols **38b**. Nitrophenol **40** was first alkylated with benzyl bromide in the presence of potassium carbonate to give compound **41** and then was converted to intermediates **42a**, as described earlier. Hydrogenation of intermediates **42a** with ammonium formate in the presence of Pd/C produced phenols **38b**. Phenols **35** and **38a**,**b** were alkylated with alkyl halides in the presence of cesium carbonate to afford the desired final products **36** (entries **101**−**104**, Table 3) and **39** (entries **119**−**121**, Table 3). Morpholine analogues **42b** (entries **109**, **110**; Table 3) were prepared from trifluoronitrobenzene **43** upon treatment with morpholine to

Scheme 2[a]

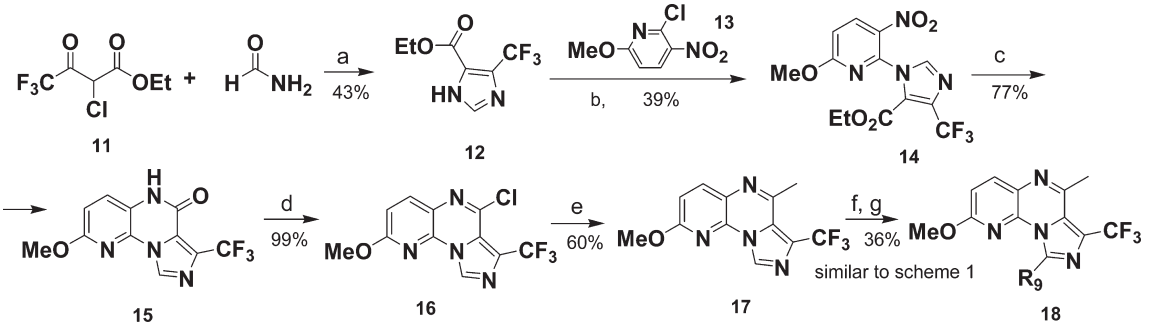

[a] Reagents: (a) H_2O; (b) KOH, DMF; (c) CH_3CO_2H, $NaHSO_3$; (d) $POCl_3$; (e) Me_3Al, $Pd(PPh_3)_4$; dioxane; (f) *N*-bromosuccinimide, CH_3CN; (g) $R_9B(OH)_2$, K_2CO_3, $Pd(PPh_3)_4$, dioxane/H_2O, 3:1.

produce **44**, which was further converted to the final products as before.

RESULTS AND DISCUSSION

Inhibitory potencies of our compounds were tested using in vitro inhibition of human recombinant PDE10A catalyzed cAMP hydrolysis. The results are compiled in Tables 1−3.

Our SAR studies encompass three key objectives. First, alter the planarity of the parent compound **1** to eliminate possible intercalation with DNA. Second, improve the metabolic stability and pharmacokinetic properties to produce drugable candidates, and third, further optimize ligand potency, selectivity, and in vivo efficacy. Examination of the X-ray crystal structure of **1**:PDE10A revealed a large unoccupied region of the ligand binding pocket (Figure 2), allowing the introduction of bulky groups at the C9 position of the parent compound to break the planarity of the tricyclic fused-ring system of **1**. Molecular modeling calculations also suggested that introduction of ortho-substituted aromatic moieties at the C9 position would produce maximum torque rotation between the aromatic groups and the fused-ring system. Such structural arrangement will alter the three-dimensional planarity of the parent structure **1**, thus preventing its alignment between the base pairs of DNA. In Tables 1−3 we have aggregated selected prepared analogues that support our SAR objectives. The *o*-tolyl analogue **46** showed potency similar to that of **1** with a modest improvement of the microsomal stability in human microsomes. The trifluoromethyl **47** and chloro **48** analogues, carrying more stable groups on the phenyl moiety, showed metabolic stability properties similar to those of **46**; nonetheless, **47** was 3-fold weaker in potency than **46**, while **48** was 3-fold more potent than **46**. The dihalogenated analogues **49** and **50** also had a metabolic stability profile similar to that of **46**. The less bulky monochloro analogue **48** was about 4-fold more potent than the dichloro analogue **49**. The alkoxy analogues **51** and **52** demonstrated an 2- to 3-fold decrease in potency (**51** and **52** vs **1**). Carboxamides **53** and **54** were the most metabolically stable analogues in both human and rodent microsomes; however, they displayed different inhibitory potency for PDE10A. The ortho analogue **53** was about 90-fold weaker than the para-substituted analogue **54**. Compound **54** exhibited a desirable in vitro profile for further in vivo evaluation; however, its high topological polar surface area (TPSA, 93 Å^2) property contributed by the polar carboxamide group resulted in poor brain permeability (<20%) with concomitant limited central drug exposure for in vivo evaluation. The phenyl analogues of Table 1 with alkyl, alkoxy, and halogen substituents had desirable TPSA values (∼50−60 Å^2) and demonstrated excellent brain permeation (>90%); however, their weak metabolic stability and short terminal half-life (about 0.5 h) excluded them from further in vivo evaluation. Analogues **46** and **49** were evaluated in the Ames test (TA98, TA100, TA1537 strains) and were found to be negative in the assay. Our initial hypothesis to introduce bulky groups at position C9 of the fused-ring system to alter the planarity of the parent molecule has resulted in the elimination of the mutagenicity potential of this class of compounds. Despite our initial success on breaking the planarity of the core structure without loss of target affinity and selectivity, our second objective to improve the microsomal stability of the molecule has remained unresolved. As we discussed above, the C7 position methyl group of **1** was identified as a key site of metabolic instability (Figure 3). We have masked this position with a trifluoromethyl moiety, which is resistant to metabolic oxidation, in an attempt to improve the compound's metabolic stability. All prepared trifluoromethyl analogues **55**−**60** were metabolically stable in both human and rodent microsomes; however, their potency for PDE10A was markedly reduced by about 10- to 20-fold compared to the C7 position methyl substituted analogues **46**−**50**. Considering that the methyl and trifluoromethyl groups are comparable in size, unfavorable electrostatic repulsions between the trifluoromethyl group of the ligand and the closely positioned residue Ser667 of the binding site are the likely cause of potency loss. Next, we investigated the C6 position of **1**, where the methyl group is prone to metabolic oxidation (Figure 3). Replacement of the C6 methyl group of **1** with a trifluoromethyl group (**61**) resulted in about 30-fold loss of potency, while the difluoromethyl moiety (**62**), though comparable in size to trifluoromethyl group, exhibited potency similar to that of parent compound **1**. Both of the fluorinated analogues exhibited better microsomal stability in human microsomes than **1**. The cyano analogue **63** was also equipotent to **1**. Furthermore, replacement of the metabolically labile 2-OMe moiety of **1** (Figure 3) with either a trifluoromethoxy or difluoromethoxy group, both of which are resistant to metabolic oxidation, has resulted in retention of the PDE10A potency but without any improvement of the microsomal stability of the compound (data not shown). A multitude of C9 position substituted phenyl analogues (data not shown) with any number of substituents (alkyl, alkoxy, halogens, etc.) and various substitution patterns (ortho, meta, para, and combinations) were prepared and tested against all PDEs. The

dx.doi.org/10.1021/jm2009138 |*J. Med. Chem.* 2011, 54, 7621–7638

Table 3. Phenylpyrazine Analogues

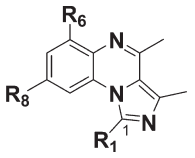

				IC$_{50}$ (nM)[a]		
compd	R_1	R_6	R_8	PDE10A	PDE2	microsomal stability, h/r, $t_{1/2}$ (min)[b]
81	3-(4-Me-pyridine)	H	H	113 ± 7.7		>30/26
82	3-(4-Me-pyridine)	H	F	158 ± 6.4		>30/>30
83	4-(3-Me-pyridine)	H	F	49.2 ± 2.6		>30/14
84	2-Me-Ph	H	F	14.4 ± 0.3	75 ± 5.8	25/3
85	3-(4-Me-pyridine)	H	Cl	28.9 ± 4.3	40 ± 2.3	>30/24
86	4-(3-Me-pyridine)	H	Cl	11 ± 1.7	14 ± 1.7	27/14
87	3-(4-Me-pyridine)	H	OMe	24.2 ± 1.1	89 ± 1.8	25/10
88	3-(4-Me-pyridine)	H	OCF_3	46 ± 5.9		23/22
89	4-(3-Me-pyridine)	H	OCF_3	8.3 ± 0.7	23 ± 4.5	>30/12
90	3-(4-Me-pyridine)	H	CF3	35.7 ± 3.5		>30/17
91	4-(3-Me-pyridine)	H	CF_3	7.4 ± 0.6	13.6 ± 2.0	24/15
92	3-(2 Me-pyridine)	H	CF_3	6.8 ± 0.6	14.7 ± 2.2	>30/28
93	3-(4-Me-pyridine)	F	F	79.5 ± 1.4		>30/>30
94	4-(3-Me-pyridine)	F	F	22 ± 1.5	153 ± 2.2	>30/26
95	3-(4-Me-pyridine)	OMe	F	2.0 ± 0.3	305 ± 41	>30/>30
96	4-(3-Me-pyridine)	OMe	F	0.7 ± 0.03	108 ± 17	>30/>30
97	3-(2 Me-pyridine)	OMe	F	0.55 ± 0.07	92 ± 16.7	>30/>30
98	2,4-Me,Me-thiazole	OMe	F	1.5 ± 0.1	621 ± 78.4	>30/>30
99	*N*-Me,3,5-Me,Me-pyrazole	OMe	F	0.85 ± 0.12	194 ± 22.3	>30/>30
100	2-Me-Ph	OMe	F	0.35 ± 0.03	66 ± 2.4	>30/26
101	2-Me-Ph	$OCHF_2$	F	1.9 ± 1.3	138 ± 24.6	18/5
102	2-Me-Ph	OCH_2CH_3	F	7.5 ± 0.9	300 ± 66.9	15/5
103	2-Me-Ph	OCH_2CF_3	F	11.4 ± 1.5	619 ± 65	>30/8
104	2-Me-Ph	OCH_2-cyclopropane	F	102 ± 4.8		12/6
105	2-Me-Ph	OH	F	63.9 ± 7.0		6/6
106	3-(4-Me-pyridine)	OMe	OMe	0.5 ± 0.05	165 ± 18.8	>30/16
107	4-(3-Me-pyridine)	OMe	OMe	0.2 ± 0.02	83 ± 10.5	25/13
108	3-(2 Me-pyridine)	OMe	OMe	0.14 ± 0.01	30 ± 3.9	>30/27
109	4-(3-Me-pyridine)	OMe	morpholine	1.7 ± 0.2	501 ± 50	>30/26
110	3-(2 Me-pyridine)	OMe	morpholine	0.1 ± 0.01	42 ± 4.9	>30/>30
111	3-(2 Me-pyridine)	OMe	OCH_2Ph	0.05 ± 0.01		3/3
112	3-(2 Me-pyridine)	OMe	$OCHF_2$	0.06 ± 0.01	71 ± 7.8	>30/>30
113	4-(3-Me-pyridine)	OMe	CF3	0.09 ± 0.01	112 ± 9.1	>30/>30
114	4-(3-Me-pyridine)	Cl	OMe	0.8 ± 0.1	411 ± 22.6	>30/14
115	4-(3-Me-pyridine)	Cl	CF3	0.7 ± 0.03	325 ± 21	>30/17
116	3-(4-Me-pyridine)	F	OMe	11.7 ± 1.8	70 ± 6.5	>30/>30
117	4-(3-Me-pyridine)	F	OMe	3.9 ± 0.3	70.5 ± 10.6	17/15
118	3-(2 Me-pyridine)	F	OMe	1.5 ± 0.2	21.6 ± 2.1	>30/28
119	4-(3-Me-pyridine)	F	$OCHF_2$	3.5 ± 0.1	36 ± 1.2	>30/20
120	4-(3-Me-pyridine)	F	OCH_2CF_3	5.5 ± 0.5	128 ± 4.6	>30/>30
121	4-(3-Me-pyridine)	F	OCH_2-cyclopropane	5.7 ± 0.3	81 ± 2.1	18/9
122	*N*-Me,3,5-Me,Me-pyrazole	F	OMe	2.9 ± 0.3	22 ± 2.3	>30/>30

[a] Mean of IC$_{50}$ with standard error of the mean; n = 4. [b] h = human. r = rat.

potency, selectivity, and metabolic stability of these new analogues were similar to those of the above-discussed ortho analogues. We have routinely evaluated the selectivity profile of all prepared compounds against all PDEs isoforms. All tested

dx.doi.org/10.1021/jm2009138 |*J. Med. Chem.* 2011, 54, 7621–7638

Scheme 3[a]

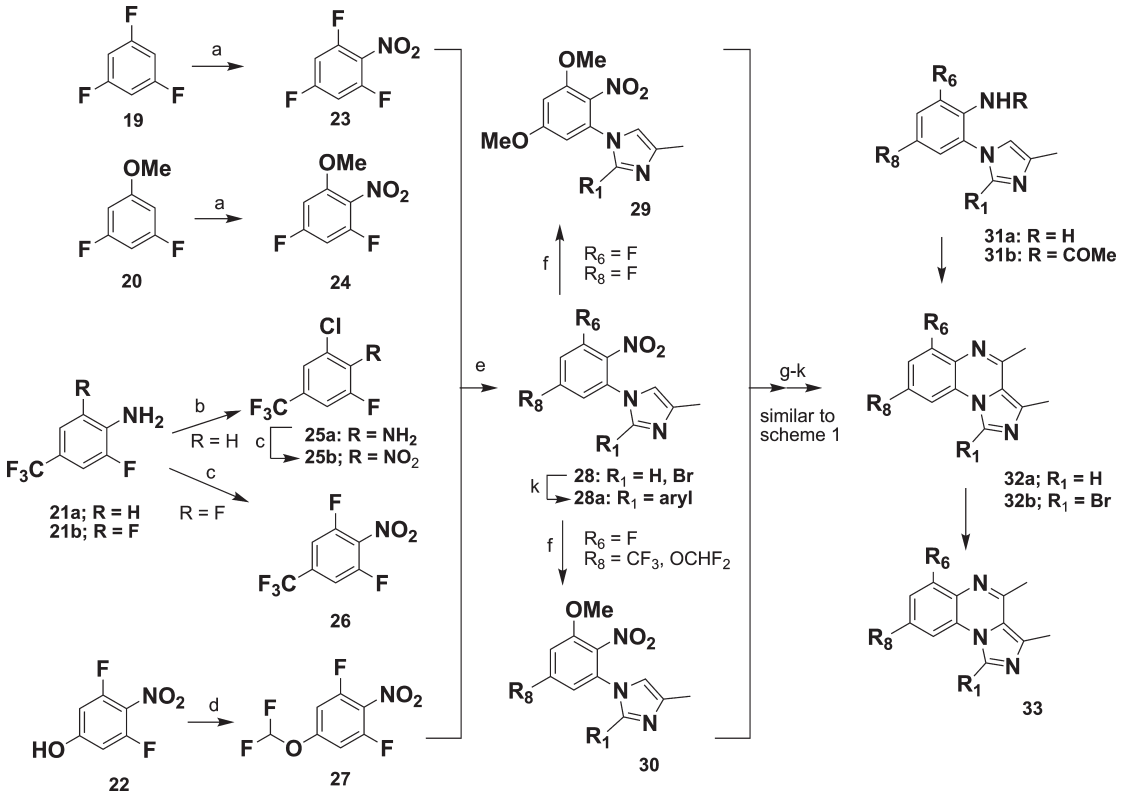

[a] Reagents: (a) HNO_3, CH_2Cl_2; (b) *N*-chlorosuccinimide, CH_3CN; (c) $NaBO_3.H_2O$, CH_3CO_2H; (d) $PhCOCClF_2$, KOH or ClF_2CO_2Na; (e) 2-bromo-4-methylimidazole or 4-methylimidazole, K_2CO_3, DMF; (f) KOH, MeOH; (g) Pd/C, HCO_2NH_4, MeOH; (h) AC_2O, toluene; (i) P_2O_5, $POCl_3$; (j) *N*-bromosuccinimide, CH_3CN; (k) $R_1B(OH)_2$, K_2CO_3, $Pd(PPh_3)_4$, dioxane/H_2O 3:1.

compounds have demonstrated high selectivity (>500−1000×; data not shown) for all PDEs isoforms with the exception of the PDE2 isoform. For matter of brevity, we are presenting our SAR evolution only with respect to PDE10A and PDE2 activity. However, if unexpected findings emerged during the screening against the other PDEs, we present these data appropriately.

Next, we turned our attention to the evaluation of heteroaryl groups at position C9. The thienyl analogue **64** was 3-fold more potent than **46**, while the *N*-Me pyrrole **65** and pyrazole **66** were 2-fold weaker in potency than **46**. Both of these new analogues were metabolically unstable. In contrast, the methyl-substituted pyrazoles **67** and **68** exhibited high resistance to metabolic oxidation and were stable in both human and rodent microsomes (**67**, **68** vs **66**). Steric interactions between the bulkier ligands, where the C9-group projects off the plane of the fused-ring core scaffold, and the cytochrome P450 degrading proteins are likely the cause of the decreased metabolic activity, with concomitant increase in compound metabolic stability. Similar to the substituted pyrazoles, both substituted isoxazole **69** and thiazole **70** also exhibited enhanced metabolic stability in human microsomes. Pyrimidine **71** showed weak PDE10A potency and moderate stability (**71** vs **46**), while pyridine **72** was 5-fold more potent than **71**. Introduction of a methyl moiety at the ortho position on the C9 pyridine nucleus to increase its size and maximize rotation in relation to the fused-ring system resulted in a 3-fold increase in potency (**73** vs **72**). The para-methyl substituted pyridine **75** was 18-fold less potent and metabolically unstable (**75** vs **73**). The para-methyl group most likely generates a steric conflict with residues at the wall of the binding pocket, which contributes to the marked loss in ligand affinity. The chloro analogue **76** has retained the PDE10A potency, but it was metabolically less stable (**76** vs **74**). The para-pyridine **77** was 2-fold more potent that the meta-pyridine **74**. Introduction of an ortho chlorine substituent (entry **78**) resulted in potency retention but with pronounced microsomal instability (**78** vs **77**). One can hypothesize that chlorine's electron-withdrawing effect reduces the electronic richness of the pyridine nucleus (entries **76** and **78**), which likely affects the binding affinity between the ligand and cytochrome P450 oxidizing proteins, thus influencing their microsomal stability. The methoxy-substituted pyridines **79** and **80** exhibited potency and stability similar to those of the methyl analogues **73** and **74**. Compounds **68** and **74** were selected for evaluation in the Ames test (TA98, TA100, TA1537 strains) and were found to be negative in the assay. All prepared heteroaryl analogues had desirable TPSA values (∼55−65 $Å^2$) and demonstrated excellent brain permeability (>90%). In order to unambiguously confirm the orientation of the C9 aromatic moiety, we have crystallized compound **74** with human PDE10A protein. Examination of the **74**:PDE10A crystal structure (Figure 4) revealed that the C9 pyridine projects toward the opened space of the PDE10A binding pocket, in agreement with our molecular modeling calculations, and it is positioned practically in a vertical orientation relative to the fused-ring system. This orientation breaks the overall three-dimensional planarity of the parent compound **1** and restricts basically the insertion of the ligand between the base pairs of DNA. Furthermore, the fused ring

dx.doi.org/10.1021/jm2009138 |*J. Med. Chem.* 2011, 54, 7621–7638

Scheme 4[a]

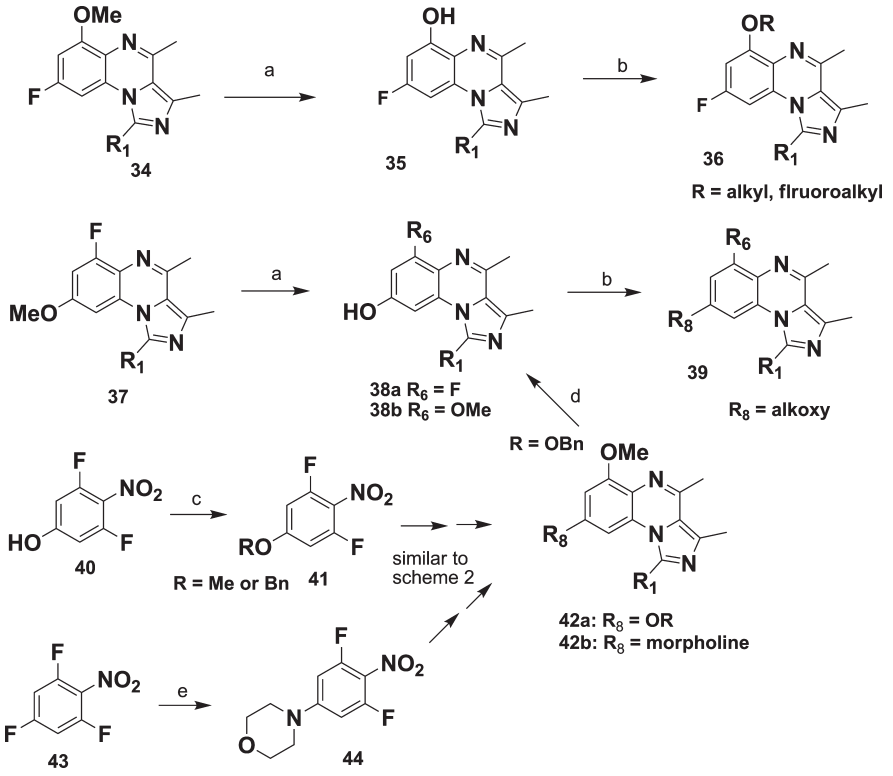

[a] Reagents: (a) BBr_3, $ClCH_2CH_2Cl$; (b) Cs_2CO_3, alkyl halides; (c) $PhCH_2$ Br or MeI, K_2CO_3; (d) HCO_2NH4, Pd/C; (e) morpholine.

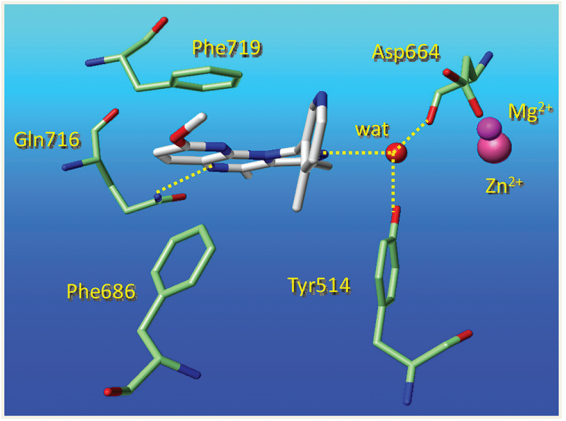

Figure 4. Crystal structure (1.9 Å resolution) of PDE10A complexed with **74**, highlighting the key hydrogen-bonding interactions between ligand and protein at the invariant Glu716, and the water-mediated contacts with Asp664 and Tyr514. The fused ring system of the ligand is sandwiched between residues Phe719, Ile682, and Phe686, making π-stacking interactions with Phe719, π-edge stacking with Phe686, and hydrophobic contact with Ile682 (not shown). The C9 position methylpyridine rotates off the fused tricyclic ring system at about 90°.

system of the ligand is sandwiched between residues Phe719, Ile682, and Phe686, making π-stacking interactions with Phe719 and hydrophobic contacts with residues Ile682 and Phe686. Also, the ligand extends toward the invariant Glu716 residue and makes a hydrogen-bonding interaction between the pyrazine nitrogen and Glu716. The ligand is further stabilized within the binding pocket with additional water-mediated hydrogen bonding interactions between the imidazole nitrogen and the residues Tyr514 and Asp664. Compounds **68** and **74** have displayed desirable in vitro and ADME profiles and were selected for further in vivo evaluation. Both compounds were efficacious in well-established predictive animal models for the positive symptoms of schizophrenia, namely, the reversal of MK-801 induced locomotor activity (LMA, Table 5) and conditioned-avoidance responding (CAR; MED values of 3 mg/kg, po, rat) assays. The pharmacokinetic profiles of **68** and **74** in rats (Table 4) and dogs have shown moderate clearance, low volume of distribution, good bioavailability in rats (**68**, 67%; **74**, 45% po 2.5 mg/kg) and dogs (**74**, 100% po 2 mg/kg), and rather short terminal half-lives in rats (0.5 h) and dogs (1 h). Despite the robust metabolic stability of **68** and **74** in both rodent and human microsomes, in vivo metabolic studies have revealed that the 2-OMe pyridine group was extensively demethylated after oral administration to form a 2-pyridone moiety. The in vivo extensive metabolism of **68** and **74** most likely has contributed to the rapid elimination of the compounds and short terminal half-life, especially in rodents. Armed with this information, we developed a chemistry strategy to replace the 2-OMe pyridine moiety of **74** with a substituted phenyl moiety in an attempt to reduce metabolism and improve the pharmacokinetic properties of the compound. In parallel, we envisioned expanding the SAR studies of **74** and improving its potency and selectivity for PDE10A. Examination of the **74**: PDE10A X-ray crystal structure (Figure 4) revealed that addition of an electron rich group at C4 position of **74** offered the potential for additional interactions between the ligand and the invariant residue Glu716. To delineate these observations, we

dx.doi.org/10.1021/jm2009138 |J. Med. Chem. 2011, 54, 7621–7638

Table 4. Selectivity of Representative Compounds toward Human PDEs Isoforms

	IC_{50} (nM)[a]										
compd	PDE1	PDE2	PDE3	PDE4	PDE5	PDE6[b]	PDE7	PDE8	PDE9	PDE10	PDE11
1	>5000	270 ± 17.6	>5000	>5000	920	>1000	3345	>5000	>5000	7.3 ± 0.6	690
49	>1000	11 ± 1.9	>1000	>1000	>1000	>1000	332	>1000	>1000	7.4 ± 0.7	>1000
50	>1000	27.5 ± 3.8	>1000	>1000	>1000	>1000	1300	>1000	>1000	4.3 ± 0.4	>1000
54	>10000	37 ± 4.6	>5000	>10000	2080	1870	2930	>10000	>10000	1.8 ± 0.2	2810
46	>5000	47 ± 7.5	>10000	>10000	1240	3100	542	>10000	>1000	7.5 ± 0.7	2400
64	>5000	62 ± 6.5	6900	6350	1440	1780	266	>10000	>10000	2.8 ± 0.1	1510
68	>10000	24.6 ± 1.9	>10000	>10000	>10000	>10000	1170	>10000	>10000	6.1 ± 0.5	>10000
70	>10000	30 ± 5.6	5280	2590	3110	1330	824	>10000	>10000	3.7 ± 0.3	5090
74	>10000	38 ± 6.4	2680	>10000	1850	1630	2318	>10000	>10000	11 ± 1.1	>10000
89	>5000	23 ± 4.5	>5000	>10000	>10000	>10000	919	>10000	>10000	8.3 ± 0.7	5290
91	>5000	14.7 ± 2.2	>5000	>5000	>1000	>5000	1340	>5000	>5000	6.8 ± 0.6	>5000
96	>10000	108 ± 17	>10000	>10000	>5000	>5000	>100000	>10000	>10000	0.7 ± 0.03	>10000
97	>10000	92 ± 16.7	>10000	>5000	5165	13700	>10000	>10000	>10000	0.55 ± 0.07	2200
106	>10000	165 ± 18.8	>10000	>10000	8780	3570	>10000	>10000	>10000	0.5 ± 0.05	4870
107	>10000	83 ± 10.5	>10000	>10000	>5000	3440	>10000	>10000	>10000	0.2 ± 0.02	3350
108	>10000	30 ± 3.9	>10000	2650	2050	2300	>10000	>10000	>10000	0.14 ± 0.01	2350
113	>500	112 ± 9.1	>500	>500	>500	>500	>500	>500	>500	0.09 ± 0.01	>500
114	>1000	411 ± 22.6	>1000	>1000	>1000	>1000	>1000	>1000	>1000	0.8 ± 0.1	>1000
115	>1000	325 ± 21	>1000	>1000	>1000	>1000	>1000	>1000	>1000	0.7 ± 0.03	>1000

[a] Mean of IC_{50} with standard error of the mean; $n = 4$. IC_{50} values are related to the maximum concentration used in the screen. [b] Bovine isoform.

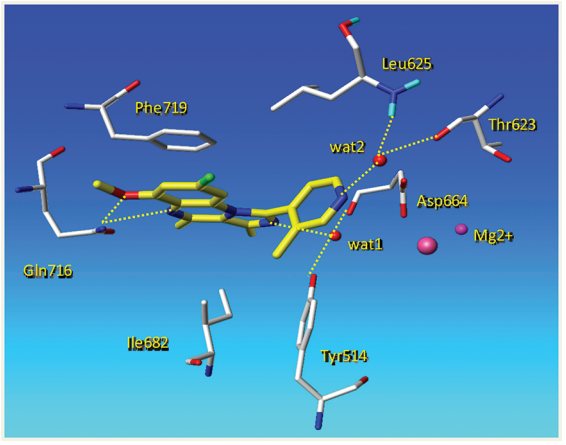

Figure 5. Crystal structure (1.8 Å resolution) of PDE10A complexed with **96**, highlighting the key hydrogen-bonding interactions between ligand and protein at the invariant Glu716 with both the pyrazine nitrogen and the 6-OMe group, and the two water-mediated contacts with Asp664, Tyr514, Thr623, and Leu625. The additional contacts between the 6-OMe and Glu716 and the water-mediated interactions with Thr623 and Leu625 contribute to the ligand's increased affinity for PDE10A.

have designed an alternative scaffold (Table 3) by replacing the pyridine nucleus with a phenyl group while maintaining at the C1 position of the new scaffold the same pyridine groups we have optimized above for PDE10A potency and microsomal stability. The initial phenyl analogues **81**−**83** were weak against PDE10A, with the C1 position substituted para-pyridine **83** being about 3-fold more potent than the analogous meta-pyridine **82**. The toluene analogue **84** was about 10-fold better than **82**, but metabolically it was unstable. Employing a variety of electron withdrawing and electron donating groups (entries **85**−**94**) at position C8 resulted in about 5- to 10-fold enhancement of the PDE10A potency, which was comparable to that of the pyridine−pyrazine analogues as described above. The phenylpyrazine analogues demonstrated a 3- to 5-fold potency difference between para- and meta-substituted C1 pyridines (**88** vs **89**, **90** vs **91**, **93** vs **94**). The increased potency of the C1 substituted para-pyridines is due to the additional water-mediated hydrogen-bonding interaction between the pyridine nitrogen and residues Leu623 and Thr623 (supportive X-ray crystallography findings are shown below in Figure 5). Next, we turned our attention to the C6 position of **74**, where molecular modeling calculations and X-ray observations with the **74**:PDE10A crystal structure have suggested that electron donating groups at the C6 position offered the potential of new contacts between the ligand and residue Glu716. Introduction of a methoxy moiety at position C6 (entry **95**) resulted in about 80-fold improvement of the PDE10A potency (**95** vs **82**). In addition, the para- and ortho-pyridines **96** and **97** exhibited exceptional potency for PDE10A, representing our first compounds with subnanomolar affinity for PDE10A. The thiazole and pyrazole analogues **98** and **99** were also very potent PDE10A inhibitors. To confirm our molecular modeling calculations, compound **96** was crystallized with human PDE10A. Examination of the **96**:PDE10A X-ray crystal structure (Figure 5) revealed that the ligand orients into the binding pocket similarly to that of compound **74**, with two additional hydrogen-bonding interactions: (i) those between the C6 methoxy group of **96** and the invariant Glu716; (ii) water-mediated contacts between the pyridine nitrogen of the ligand and the residues Thr623 and Leu625 of the binding pocket. All other observed contacts between the ligand and residues of the ligand binding pocket were similar to the contacts observed in the **74**:PDE10A X-ray crystal structure. Next, we explored the size and electronic

dx.doi.org/10.1021/jm2009138 |J. Med. Chem. 2011, 54, 7621–7638

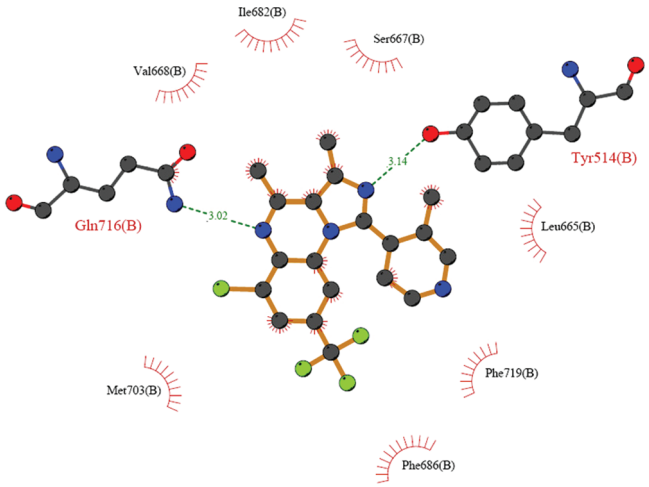

Figure 6. Ligplot[23] representation (2.4 Å resolution) of PDE10A complexed with **115**, highlighting the hydrophobic and hydrogen bond interactions between the ligand and the amino acid residues involved in the PDE10A binding pocket. The ligand orients into the binding pocket similarly to that of compound **96** (Figure 5), making several hydrophobic contacts; however, the presence of the C6-chloro substituent has caused a slight shift of the ligand within the binding pocket, causing direct interaction with residue Tyr514.

requirements of C6 substitution toward potency. The difluoromethoxy analogue **101** was 6-fold weaker than the methoxy analogue **100**. Since the difluoromethoxy moiety is practically equal in size to that of the methoxy group, the increased electronegativity of the difluoromethoxy group is likely the cause of potency loss. One can hypothesize that either the reduced electronic environment of the oxygen atom attached to the difluoromethyl electronegative group weakens the hydrogen-bond interaction between the difluoromethoxy group and the NH functionality of the Glu617 residue or the electronegative difluoromethoxy group creates an electronic repulsive environment with Glu716. Increasing the size of the C6 group has affected the ligand's potency. Ethoxy analogue **102** was 20-fold less potent than **100**, while the more electronegative trifluoroethoxy analogue **103** was even less potent (40-fold, **103** vs **100**). The bulkier cyclopropane analogue **104** was markedly 400-fold less potent (**104** vs **100**). Bulky groups are likely restricting the hydrogen-bond contact between the ligand's pyrazine nitrogen and Glu716 and causing the realignment of the ligand within the binding pocket, which results in marked loss of the ligand's affinity. Demethylation of the C6 methoxy group (entry **105**) resulted in 200-fold loss of potency. To further expand the breadth of our SAR studies, we explored C8 position substitutions (**106**−**112**). Introduction of a methoxy moiety at C8 resulted in about 3-fold improvement of the PDE10A potency (**108** vs **97**). The bulkier morpholine **110** and benzyl analogues **111** were also very potent (**110**, **111** vs **97**). Even though the C8 methoxy analogues showed good metabolic stability, in vivo metabolic studies indicated that the C8 methoxy group of **106** was prone to demethylation, resulting in a short terminal half-life (rat $t_{1/2}$ ≈1.5 h) after oral administration. Replacing the C8 methoxy group with the more stable difluoromethoxy and trifluoromethoxy moieties (entry **112**, **113**) resulted in (i) about 2-fold increase in potency (**112** vs **108**), (ii) enhancement of the microsomal stability, and (iii) longer elimination half-life in rats (**112** $t_{1/2}$ ≈ 3.5 h and **113** $t_{1/2}$ ≈ 11.7 h, respectively). Finally, we have replaced the C6 methoxy group with fluorine and chlorine substituents while maintaining at the C8 position the above optimized substituents (**114**−**122**). All analogues were about 3- to 20-fold less potent than the analogous C6-methoxy analogues (**114** vs **107**, **117** vs **97**). The unexpected high potency of the C6-chloro analogue **115** (**115** vs **89**), considering that the addition of an electron donating methoxy group at C6 was a prerequisite to the ligand's high affinity, as discussed above (i.e **113** vs **89**), prompted us to investigate this finding by crystallizing compound **115** with human PDE10A. Examination of the **115**:PDE10A X-ray crystal structure (Figure 6) revealed that the ligand orients in the binding pocket similarly to that of compound **96**; however, the presence of the C6-chloro substituent has caused a slight shift of the ligand within the binding pocket, bringing it closer to residue Tyr514. This ligand realignment within the binding pocket has triggered the displacement of the conserved water, present in the previous **96**:PDE10A X-ray crystal structure, promoting a direct contact between the ligand and residue Tyr514. The gained binding energy of the direct hydrogen-bond interaction between the ligand and residues Tyr514 is likely the cause of the increased ligand affinity. The direct contact between ligand and protein favorably compensates for the loss in desolvation energy necessary to displace the conserved water. Most of the other contacts between the ligand and PDE10A protein were similar to the above-discussed X-ray crystal structures.

All tested compounds have demonstrated high selectivity for all PDEs with the exception of PDE2, where a lower level of selectivity was observed. Nevertheless, the C6,C8-disubstituted phenyl analogues (i.e., entries **106**, **112**−**115**), which have exhibited subnanomolar affinity for PDE10A, have demonstrated high selectivity (>500×) against PDE2. Table 4 outlines a collection of representative analogues that were evaluated against the PDE panel of human isoforms, with the exception of PDE6 which is the bovine isoform.

The selectivity of key analogues **68**, **96**, and **106** was assessed in Nova Screen assays (neurotransmitters, ion channels, growth factors/hormones, kinases, brain/gut peptides, immunological factors, and prostaglandins). All compounds were devoid of any activity at 10 μM in all tested assays, with the exception of **96** which showed activity against adenosine A1 (IC_{50} = 150 nM) and A2A (IC_{50} = 5.05 μM).

Most of the analogues shown in Table 3 have demonstrated good microsomal stability in both human and rodent microsomes, have desirable TPSA values (∼50−65 Å^2), and exhibit excellent brain permeability (>90%). The robust brain permeability of this class of compounds was indicative of the molecule's low molecular weight, low topological surface area, and lack of P-glycoprotein (P-gp) mediated efflux property. Evaluation of the PDE10 inhibitors in the MDR1-MDCK permeability assay revealed that the compounds, while showing a high level of permeability [apical to basolateral (A−B) P_{app} and basolateral to apical (B−A) P_{app}], lacked efflux properties (data not shown).

The pharmacokinetic properties of several compounds in rats and dogs after oral administration are summarized in Table 5. All compounds showed low to moderate clearance, low volume of distribution, good bioavailability in rats and dogs, low to good terminal half-lives (especially for the later phenylpyrazines), and good brain exposure.

Effect of PDE10A Inhibition on Striatal Cyclic Nucleotide cAMP and cGMP Levels in Vivo. Given the dual nature of PDE10A phosphodiesterase activity, we have examined the effect of PDE10A inhibitor **96** in vivo by assessing striatal cAMP and

Table 5. Pharmacokinetic Profile of Selected Compounds

	68	74	96		106		112	
	rat	rat	rat	dog	rat	dog	rat	dog
dose (mg/kg)	2.0	2.5	2.5	2.5	2.5	2	0.1	0.5
F (%)	67	25	27	73	25	100	83	84
$t_{1/2}$ (h)	0.5	0.5	1.5	1.8	1.3	3.4	3.5	3.0
CL (mL min^{-1} kg^{-1})	10	31	14	38	14	8	7	6
V_{ss} (L/kg)	0.7	1	0.9	6	1.3	1.6	0.6	1.1
AUC_{brain}/AUC_{plasma},[a] 10 mg/kg po	2941/4128	866/747	2372/3638	nt	3279/8852	nt	4400/12738	nt

[a] AUC in h·ng/mL.

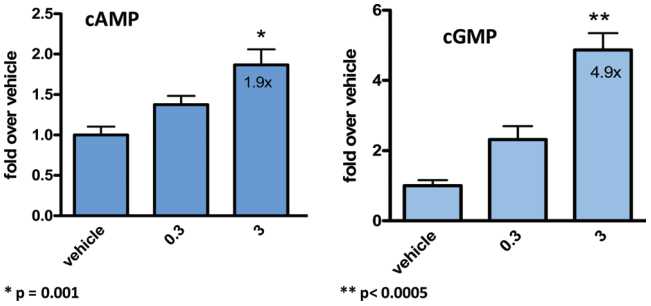

Figure 7. Dose-dependent effects of **96** upon mouse striatal cyclic nucleotide levels. Compound **96** was administered 10 or 30 min before sacrifice (n = 4): vehicle-treated; *, p = 0.001; **, p < 0.0005.

cGMP tissue levels after dosing with the compound. Compound **96** showed excellent potency (PDE10A IC_{50} = 0.7 nM) and selectivity (>3000× against PDE1, PDE3−9, PDE11; >150× against PDE2). The effect of dosing compound **96** (0.3 and 3.0 mg/kg, ip, 30 min) in CF-1 mouse on striatal cyclic nucleotides was assessed. Dose-dependent increases in both cAMP and cGMP levels were observed with statistically significant changes of 1.9- and 4.9-fold in the levels of cAMP and cGMP, respectively, over the vehicle-treated animals with the 3 mg/kg dose (Figure 7). A study of enzyme occupancy with **96** (unpublished data) indicated about approximately 80% occupancy was required to achieve these cyclic nucleotide elevations.

Effect of PDE10A Inhibitors in Models Predictive of Antipsychotic ActivityReversal of MK-801 Induced Hyperactivity in Rats. A representative subset of high affinity PDE10A inhibitors was selected for investigation of their antipsychotic-like potential in vivo. To enable the characterization of the antipsychotic activity, we utilized a MK-801 induced hyperactivity reversal model. MK-801 (0.1 mg/kg ip) significantly increased horizontal activity (t test, p < 0.001) and induced stereotyped sniffing (t test, p < 0.001) in female rats. These behaviors were significantly reversed by the positive control, which in this case was the atypical antipsychotic clozapine. All evaluated PDE10A inhibitors also reversed hyperactivity and stereotyped sniffing in a dose dependent and significant manner. The minimal effective dose (MED) of the novel PDE10A inhibitors can be seen in Table 6. There is a clear qualitative correlation between in vitro potency at PDE10A and MED values in this assay, with the most potent phenylpyrazines (**96**, **106**, **108**, **112**, **113**) representing the most efficacious in vivo analogues.

Disruption of Conditioned Avoidance Responding (CAR) in Rats. Disruption of the "avoidance" response in CAR is another preclinical model predictive of antipsychotic activity. In the rat CAR model (Figure 8), **96** decreased avoidance responding with a significant treatment effect at 1 mg/kg. Data are expressed as mean (with SEM) avoidance, escape, and response failures observed over 50 trials (n = 8 animals/group). Nonlinear regression analysis calculated an ID_{50} equivalent to 1.19 ± 0.29 mg/kg; p = 0.05.

In summary, we have described the evolution of new phenylpyrazine PDE10A inhibitors based on our previously reported pyridyl-pyrazine **1**. Applications of structure-based drug design techniques and molecular modeling have led to the identification of subnanomolar PDE10A inhibitors with excellent selectivity against the other members of the PDE family. Exploring the C9 position of **1**, we were able to alter the planarity of the parent compound and eliminate a potential risk of mutagenicity. Also, the identification of a second hydrogen-bond interaction between the ligand and the invariant residue Glu716 has led to a marked increase of the ligand's affinity. A systematic assessment of the ADME and pharmacokinetic properties of the newly synthesized compounds has led to the design of several druglike candidates with high brain permeability and desirable drug kinetics ($t_{1/2}$, bioavailability, clearance). Direct correlation of PDE10A inhibition and in vivo functional activity, as assessed by cyclic nucleotides level changes, was demonstrated with **96**. Both striatal cAMP and cGMP levels were increased by 1.9× and 4.9×, respectively, at a 3 mg/kg oral dose. Compound **96** was highly potent for PDE10A (IC_{50} = 0.7 nM), demonstrated high selectivity (>3000×) for the other PDEs, with the exception of PDE2 (150× selective), and was efficacious in animal models of psychoses; reversal of MK-801 induced hyperactivity and conditioned avoidance responding (CAR).

■ EXPERIMENTAL SECTION

Chemistry. Melting points were determined in open capillary tubes on a Mel-Temp II apparatus and reported uncorrected. ^{1}H NMR spectra were determined in the cited solvent on a Varian Unity or Varian Inova (300−400 MHz) instrument with tetramethylsilane as an internal standard. Chemical shifts are given in ppm, and coupling constants are in hertz. Splitting patterns are designated as follows: s, singlet; br s, broad singlet; d, doublet; t, triplet; q, quartet; m, multiplet. Mass spectra were recorded on a Micromass LCT, Waters, spectrometer. Elemental analyses (C, H, N) were performed on a Perkin-Elmer 240 analyzer, and all compounds are within ±0.4% of theory unless otherwise indicated. HPLC techniques and high resolution mass spectrometry were used to determine the purity of compounds outside the range of the elemental analysis assessment. Purity of all final products was >96% as determined by HPLC and/or combustion analysis. Purity was determined by HPLC

dx.doi.org/10.1021/jm2009138 |J. Med. Chem. 2011, 54, 7621–7638

Table 6. Reversal of MK-801 Induced Hyperactivity and Stereotyped Sniffing

compd	MED[a] hyperactivity (mg/kg po)	% decrease in hyperactivity[b]	MED[a] sniffing (mg/kg po)	% decrease in sniffing[b]	IC_{50} (nM)[c]
68	0.5	57.4	0.1	25.1	6.1
74	1	38.2	2.5	83.5	11
96	0.075	62.4	0.075	42.6	0.7
106	0.05	39.3	0.05	25.2	0.5
108	0.0125	30.4	0.025	43.6	0.1
112	0.025	34.8	0.025	23.7	0.06
113	0.01	33.2	0.01	16.8	0.09
115	0.25	51.1	0.25	31.9	0.7
clozapine	20	16.53	20	16.28	ni[d]

[a] Minimal effective dose that significantly reduced MK-801-induced hyperactivity or stereotyped sniffing, respectively ($p < 0.05$). [b] $p < 0.001$, $n = 6$. [c] Inhibition of PDE10 activity from Tables 1−3. [d] ni: no inhibition at PDE10.

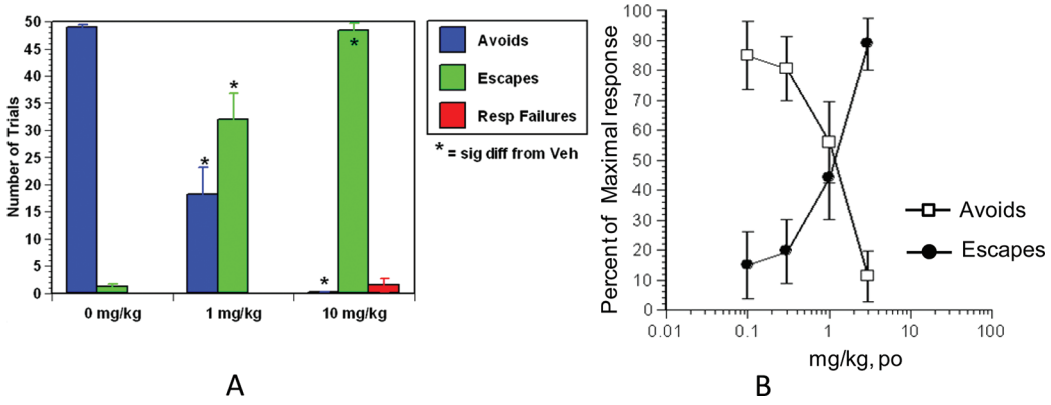

Figure 8. Compound **96** was evaluated in the conditioned avoidance response in male Sprague−Dawley rats using a 60 min pretreatment interval and an oral route of administration. Data are expressed as mean (with SEM): (A) avoidance, escape, and response failures observed in over 50 trials ($n = 8$ animals/group); ∗, statistical difference in avoidance and escape response from vehicle-treated controls ($p = 0.05$). Nonlinear regression analysis (B) calculated an ID_{50} equivalent to 1.19 ± 0.29 mg/kg; $p = 0.05$.

analysis using the following protocols. Method A: mobile phase A, H_2O (0.1% HCOOH); mobile phase B, CAN (0.1% HCOOH); solvent gradient 85/15 to 5/95 A/B in 2 min, hold 1.25 min, re-equilibrate 0.5 min; flow rate 1.8 mL/min; Onyx Monolithic C18, 0.3 cm × 10 cm; temperature 40 °C; detection at 210−370 nm. Method B: mobile phase A, 10 mM ammonium formate in water (pH 3.5); mobile phase B, 50:50 ACN/MeOH; solvent gradient 85/15 to 5/95 A/B in 2 min, hold 1.25 min, re-equilibrate 0.5 min; flow rate 1.1 mL/min; column Agilent SB C18 1.8 μm, 3.0 cm × 50 mm; temperature 45 °C; detection at 210−370 nm. All products, unless otherwise noted, were purified by "flash chromatography" with use of 220−400 mesh silica gel. Thin-layer chromatography was done on silica gel 60 F-254 (0.25 mm thickness) plates. Visualization was accomplished with UV light and/or 10% phosphomolybdic acid in ethanol. The hydration was determined by the Karl Fischer titration, using a Mitsubishi moisture meter model CA-05. Unless otherwise noted, all materials were obtained commercially and used without further purification. All reactions were carried out under an atmosphere of dried argon or nitrogen.

Representative Synthetic Protocols of the Aminohydantoins Shown in Schemes 1−4. 8-Methoxy-4-methyl-3-trifluoromethyl-2,5,9,9*b*-tetraaza-cyclopenta[*a*]naphthalene (17). *Step a. 5-Trifluoromethyl-3H-imidazole-4-carboxylic Acid Ethyl Ester (**12**).* Ethyl 2-chloro-4,4,4-trifluoroacetate (25 g, 0.114 mol) was combined with amidine (50 g, 1.1 mol) and water (5 mL). The mixture became warm and was heated to 130 °C for 1.5 h. The mixture was then cooled to room temperature, and 100 mL of ice−water was added. The resulting solids were collected and washed with water, then dried to give 5-trifluoromethyl-3*H*-imidazole-4-carboxylic acid ethyl ester as a brown solid (5.5 g, 23% yield). MS *m*/*e* 209 $[M + H]^+$; ^1H NMR (400 MHz, DMSO) δ ppm 8.41 (s, 1H), 5.6 (s, 1H), 4.12 (q, $J = 7.07$ Hz, 2H), 3.93 (s, 3H), 1.01 (t, $J = 7.19$ Hz, 3H).

*Step b. 3-(6-Methoxy-3-nitropyridin-2-yl)-5-trifluoromethyl-3H-imidazole-4-carboxylic Acid Ethyl Ester (**14**).* 5-Trifluoromethyl-3*H*-imidazole-4-carboxylic acid ethyl ester (5 g, 24 mmol) and 2-chloro-3-nitro-6-methoxypyridine (4.5 g, 24 mmol) were dissolved in DMF (60 mL). Into this mixture was added freshly powdered KOH (1.3 g, 24 mmol). The mixture was heated to 70 °C for 16 h, then cooled to room temperature and diluted with water. The solution was then extracted twice with ethyl acetate. The organic layers were combined and washed with water and brine and dried over $MgSO_4$. Evaporation and purification by flash chromatography on silica gel in hexane/ethyl acetate, 2:1, gave 3-(6-methoxy-3-nitro-pyridin-2-yl)-5-trifluoromethyl-3*H*-imidazole-4-carboxylic acid ethyl ester as a yellow oil (3.4 g, 39% yield). MS *m*/*e* 361.0 $[M + H]^+$; ^1H NMR (400 MHz, DMSO) δ ppm 8.76 (d, $J = 8.9$ Hz, 1H), 8.46 (s, 1H), 7.32 (d, $J = 9.04$ Hz, 1H), 4.12 (q, $J = 7.07$ Hz, 2H), 3.93 (s, 3H), 1.01 (t, $J = 7.19$ Hz, 3H).

*Step c. 8-Methoxy-3-trifluoromethyl-5H-2,5,9,9b-tetraaza-cyclopenta-[a]naphthalen-4-one (**15**).* 3-(6-Methoxy-3-nitropyridin-2-yl)-5-trifluoromethyl-3*H*-imidazole-4-carboxylic acid ethyl ester (2.9 g, 8.0 mmol) was dissolved in glacial acetic acid (45 mL). Into this mixture was added water (23 mL) followed by sodium hydrogen sulfite (10 g, 80 mmol). The mixture was heated to 105 °C for 16 h. An additional 2 g of the hydrogen sulfite is then added every 2 h until all starting material has been consumed, as indicated by TLC. The mixture was diluted with

dx.doi.org/10.1021/jm2009138 |J. Med. Chem. 2011, 54, 7621–7638

water, and the solids were filtered and collected. The solids were washed with water followed by a small amount of chloroform and dried to give 8-methoxy-3-trifluoromethyl-5*H*-2,5,9,9*b*-tetraazacyclopenta[*a*]naphthalen-4-one as a gray/white solid (1.8 g, 79% yield). MS *m*/*e* 285.1 $[M + H]^+$; ^{1}H NMR (400 MHz, DMSO) δ ppm 11.68 (s, 1H), 8.95 (s, 1H), 7.66 (d, *J* = 8.66 Hz, 1H), 6.96 (d, *J* = 8.67 Hz, 1H), 3.94 (s, 3H).

*Step d. 4-Chloro-8-methoxy-3-trifluoromethyl-2,5,9,9b-tetraaza-cyclopenta[a]naphthalene (**16**).* 8-Methoxy-3-trifluoromethyl-5*H*-2,5,9,-9*b*-tetraazacyclopenta[*a*]naphthalen-4-one (1.0 g, 3.5 mmol) was suspended in $POCl_3$ (11 mL) and heated to 120 °C for 3 h. The $POCl_3$ was removed under reduced pressure and the residue taken in water and neutralized with sodium bicarbonate. The resulting solids were filtered and collected and dried to give 4-chloro-8-methoxy-3-trifluoromethyl-2,5,9,9b-tetraazacyclopenta[*a*]naphthalene as a pale yellow solid (0.98 g, 99% yield). MS *m*/*e* 303.0 $[M + H]^+$; ^{1}H NMR (400 MHz, DMSO) δ ppm 9.36 (s, 1H), 8.33 (d, *J* = 8.81 Hz, 1H), 7.21 (d, *J* = 8.81 Hz, 1H), 4.09 (s, 3H).

*Step e. 8-Methoxy-4-methyl-3-trifluoromethyl-2,5,9,9b-tetraaza-cyclopenta[a]naphthalene (**17**).* 4-Chloro-8-methoxy-3-trifluoromethyl-2,5,9,9*b*-tetraazacyclopenta[*a*]naphthalene (0.2 g, 0.66 mmol) was dissolved in dry dioxane (4 mL). Into this mixture was added $Pd(PPh_3)_4$ (0.012 g, 5%mol) followed by trimethylaluminum (2 M/toluene; 1.6 mL, 3.3 mmol). The mixture was heated to 110 °C for 2 h and then cooled with an ice bath. Dilute HCl (2 mL) was slowly added to the mixture and then neutralized with dilute sodium hydroxide (4 mL). The reaction mixture was extracted with ethyl acetate, and the organic layers were separated and combined. The combined extracts were washed with water and brine and dried over $MgSO_4$. Evaporation and purification by flash chromatography on silica gel in hexane/ethyl acetate 10: 1 gave 8-methoxy-4-methyl-3-trifluoromethyl-2,5,9,9*b*-tetraazacyclopenta[*a*]-naphthalene as a white solid (0.12 g, 60% yield). MS *m*/*e* 283.0 $[M + H]^+$; ^{1}H NMR (400 MHz, DMSO) δ ppm 9.24 (s, 1H), 8.31 (d, *J* = 8.72 Hz, 1H), 7.18 (d, *J* = 8.84 Hz, 1H), 4.08 (s, 3H), 2.75 (s, 3H).

3,5-Difluoro-4-nitrophenol (22). Into a solution of 3,5-difluorophenol (14.08 g, 108 mmol) and dichlomethane (150 mL) was added fuming nitric acid (>90%, 15 mL) dropwise under a nitrogen atmosphere at 0 °C. After the addition, the resulting solution was stirred at 0 °C temperature for 2 h. The mixture was then poured into cold water, and the organic layer was separated. The aqueous layer was extracted with dichloromethane, and the combined organics were washed with brine and dried over magnesium sulfate. Condensation under vacuum and purification by column chromatography using 10−30% ethyl acetate in hexane provided 3,5-difluoro-4-nitrophenol as a yellow thick oil (5.1 g, 27% yield) (MS *m*/*e* 174 $[M - H]^+$; ^{1}H NMR (400 MHz, DMSO) δ ppm 11.75 (brs, 1H), 6.74 (m, 2H)) and the regioisomer 3,5-difluoro-2-nitrophenol as a yellow solid (8.0 g, 42% yield) (MS *m*/*e* 174 $[M - H]^+$; ^{1}H NMR (400 MHz, DMSO) δ ppm 12.16 (brs, 1H), 7.04 (m, 1H), 6.72 (m, 1H)).

2-Bromo-1-(3,5-dimethoxy-2-nitrophenyl)-4-methyl-1*H*-imidazole (29; R_1 = Br). *Step a. 2-Bromo-1-(3,5-difluoro-2-nitrophenyl)-4-methyl-1H-imidazole (**28**; R_1 = Br; R_6, R_8 = F).* A mixture of 1,3,5-trifluoro-2-nitrobenzene (2.2 mL, 18.6 mmol), 2-bromo-4-methylimidazole (3 g, 18.6 mmol), and K_2CO_3 (5.66 g, 41 mmol) in DMF (80 mL) was stirred at room temperature overnight. The mixture was diluted with ethyl acetate and washed with water and dried over magnesium sulfate. Evaporation and purification by column purification using 10% ethyl acetate in dichloromethane as eluent provided the product 2-bromo-1-(3,5-difluoro-2-nitrophenyl)-4-methyl-1*H*-imidazole as a yellow powder (3.18 g, 54% yield). MS *m*/*e* 317.9 $[M + H]^+$; ^{1}H NMR (400 MHz, DMSO) δ ppm 8.01−8.08 (m, 1H), 7.77−7.82 (m, 1H), 7.28 (s, 1H), 2.08 (s, 3H).

*Step b. 2-Bromo-1-(3, 5-dimethoxy-2-nitrophenyl)-4-methyl-1H-imidazole (**29**; R_1 = Br; R_6, R_8 = OMe).* Into a solution of 2-bromo-1-(3,5-difluoro-2-nitrophenyl)-4-methyl-1*H*-imidazole (2.98 g, 9.4 mmol) in MeOH (40 mL) was added freshly powdered KOH (2.5 g, 44.6 mmol) at room temperature under nitrogen. The resulting mixture was stirred at 55 °C for 2 h, cooled to room temperature, diluted with dichloromethane, and poured into water. The organic extracts were separated and dried over magnesium sulfate. Evaporation of the solvents provided 2-bromo-1-(3,5-dimethoxy-2-nitrophenyl)-4-methyl-1*H*-imidazole as an off-white solid (3.35 g, 100% yield). MS *m*/*e* 342.0 $[M + H]^+$; ^{1}H NMR (400 MHz, DMSO) δ 7.18 (s, 1H), 7.01 (s, 1H), 6.82 (s, 1H), 3.95 (s, 3H), 3.9 (s, 3H), 2.09 (s, 3H).

8-Fluoro-3,4-dimethyl-1-(3-methylpyridin-4-yl)imidazo-[1,5-*a*]quinoxalin-6-ol (35; R_1 = 3-methylpyridin-4-yl). Into a mixture of 8-fluoro-6-methoxy-3,4-dimethyl-1-(3-methylpyridin-4-yl)-imidazo[1,5-*a*]quinoxaline (200 mg, 0.595 mmol in dichloroethane (10 mL) was added boron tribromide (0.5 mL, 5.29 mmol) at 0 °C. The resulting mixture was warmed to 80 °C overnight, cooled to room temperature, quenched with aqueous K_2CO_3, and extracted with dichloromethane. The extracts were dried over anhydrous $MgSO_4$. Evaporation and purification by column purification (ethyl acetate, then 4−8% MeOH in dichloromethane) provided 8-fluoro-3,4-dimethyl-1-(3-methylpyridin-4-yl)imidazo[1,5-*a*]quinoxalin-6-ol as a light yellow powder (150 mg, 78% yield). MS *m*/*e* 323.1 $[M + H]^+$; ^{1}H NMR (400 MHz, DMSO) δ ppm 8.87 (s, 1H), 8.76 (d, *J* = 5.4 Hz, 1H), 7.80 (d, *J* = 5.3 Hz, 1H), 6.79 (dd, *J* = 10.5, 2.7 Hz, 1H), 6.15 (dd, *J* = 10.4, 1.5 Hz, 1H), 2.87 (s, 3H), 2.74 (s, 3H), 2.14 (s, 3H).

6-Methoxy-3,4-dimethyl-1-(2-methylpyridin-3-yl)imidazo-[1,5-*a*]quinoxalin-8-ol (38b; R_6 = OMe, R_1 = 2-methylpyridin-3-yl). A mixture of 8-(benzyloxy)-6-methoxy-3,4-dimethyl-1-(2-methylpyridin-3-yl)imidazo[1,5-*a*]quinoxaline (500 mg, 1.178 mmol) and Pd/C (62.7 mg, 0.059 mmol) in a 250 mL flask was vacuumed and refilled with nitrogen, and then THF (8 mL) and MeOH (8 mL) were added followed by addition of ammonium formate (371 mg, 5.89 mmol). The final mixture was stirred at 50 °C for 3 h, cooled to room temperature, and filtered through Celite. The Celite pad was washed with methanol and ethyl acetate. The filtrate was evaporated to provide 6-methoxy-3,4-dimethyl-1-(2-methylpyridin-3-yl)imidazo[1,5-*a*]quinoxalin-8-ol as an off-white powder (362 mg, 92% yield). MS *m*/*e* 335.1 $[M + H]^+$; ^{1}H NMR (400 MHz, DMSO) δ ppm 8.68 (m, 1H), 8.43 (s, 1H), 7.82 (m, 1H), 7.41 (m, 3H), 6.46 (d, *J* = 2.3 Hz, 1H), 5.95 (d, *J* = 2.3 Hz, 1H), 3.82 (s, 3H), 2.71 (s, 3H), 2.68 (s, 3H), 2.12 (s, 3H).

1,3-Difluoro-5-methoxy-2-nitrobenzene (41; R = Me). Into a mixture of 3,5-difluoro-4-nitrophenol (5.1 g, 29 mmol) and potassium carbonate (8.0 g, 58 mmol) in *N*,*N*-dimethylformamide (45 mL) was added iodomethane (2.2 mL, 34.8 mmol) at room temperature. The resulting mixture was stirred at room temperature overnight, and then most of the solvent was removed under vacuum. The residue was diluted with water and ethyl acetate. The organic layer was separated, and the aqueous layer was extracted with ethyl acetate. The combined organics were washed with brine and dried over magnesium sulfate. Condensation under vacuum and purification by column chromatography using 20% ethyl acetate in hexane provided 1,3-difluoro-5-methoxy-2-nitrobenzene as a yellow oil (4.4 g, 81% yield). MS *m*/*e* 190 $[M + H]^+$; ^{1}H NMR (400 MHz, DMSO) δ ppm 7.04 (m, 2H), 3.85 (s, 3H).

5-(Benzyloxy)-1,3-difluoro-2-nitrobenzene (41; R = Bn). Into a mixture of 3,5-difluoro-4-nitrophenol (14 g, 80 mmol) and potassium carbonate (24.2 g, 176 mmol) in *N*,*N*-dimethylformamide (150 mL) was added benzyl bromide (10.45 mL, 88 mmol) at room temperature. The resulting mixture was stirred at room temperature overnight, and then most of solvent was removed under vacuum. The residue was diluted with water and ethyl acetate. The organic layer was separated, and the aqueous layer was extracted with ethyl acetate. The combined organics were washed with brine and dried over magnesium sulfate. Evaporation under vacuum and purification by column chromatography using 20% ethyl acetate in hexane provided 5-(benzyloxy)-1,3-difluoro-2-nitrobenzene as a yellow solid (98% yield). MS *m*/*e* 264.8

$[M]^+$; ^{1}H NMR (400 MHz, DMSO) δ ppm 7.25−7.35 (m, 5H), 7.2 (m, 2H), 5.2 (s, 2H).

2-Methoxy-6,7-dimethyl-9-(4-methylpyridin-3-yl)imidazo-[1,5-*a*]pyrido[3,2-*e*]pyrazine (74). *Step a. 6-Methoxy-2-(4-methyl-1H-imidazol-1-yl)-3-nitropyridine (**3a**).* To a *N*,*N*-dimethylformamide (500 mL) solution of 4-methylimidazole (8.5 g, 103 mmol) was added freshly powdered KOH (6.72 g, 120 mmol) in two portions under N_2 at 0 °C, followed by addition of 2-chloro-6-methoxy-3-nitropyridine (18.9 g, 100 mmol). The resulting solution was warmed to room temperature and stirred for 2 h. The majority of the solvent was removed under vacuum, and the residue was diluted with water and extracted with ethyl acetate three times. The organic layer was combined and washed two times with water to remove additional dimethylformamide and dried over magnesium sulfate. The solvent was evaporated under vacuum and the residue was purified by column (15−25% gradient eluent of ethyl acetate in dichloromethane) to provide 6-methoxy-2-(4-methyl-1*H*-imidazol-1-yl)-3-nitropyridine as a yellow solid (21.9 g, 93% yield, inseparable 4:1 mixture of imidazole regioisomers). MS *m*/*e* 235.0 $[M + H]^+$; ^{1}H NMR (400 MHz, DMSO) δ ppm 8.48 (d, *J* = 8.7 Hz, 1H), 8.00 (d, *J* = 8.7 Hz, 1H), 7.18 (s, 1H), 7.01 (d, 1H), 3.97 (s, 3H), 2.12 (s, 3H).

*Step b. 6-Methoxy-2-(4-methyl-1H-imidazol-1-yl)pyridin-3-amine (**3b**).* To a mixture of 6-methoxy-2-(4-methyl-1*H*-imidazol-1-yl)-3-nitropyridine (21.4 g, 91.5 mmol) and 10% Pd/C (5.12 g, 4.58 mmol) in a 1 L round-bottom flask (connected with a condenser) was loaded 240 mL of THF, followed by slow addition of 240 mL of MeOH under N_2 with stirring. $HCOONH_4$ (34.75 g, 503.25 mmol) was added in two portions into the stirring mixture, and the final mixture was stirred at room temperature for 10 min (gas released) and then warmed to 50 °C for 1 h. The mixture was cooled to room temperature and filtered through Celite. Solvent was evaporated under vacuum to dryness to provide a clean product as an off-white powder (18.6 g, 99% yield). NMR indicated a 4:1 ratio mixture of two regioisomers with the major product (6-methoxy-2-(4-methyl-1*H*-imidazol-1-yl)pyridin-3-amine) as the desired regioisomer (confirmed by NOE studies). MS *m*/*e* 205 $[M + H]^+$; ^{1}H NMR (400 MHz, DMSO) δ ppm 7.91 (s, 1H), 7.30 (d, 1H), 7.25 (s, 1H), 6.63 (d, 1H), 4.70 (s, br, 2H), 3.70 (s, 3H), 2.13 (s, 3H).

*Step c. N-(6-Methoxy-2-(4-methyl-1H-imidazol-1-yl)pyridin-3-yl)acetamide (**4**).* To a solution of (6-methoxy-2-(4-methyl-1*H*-imidazol-1-yl)-pyridin-3-amine (8.16 g, 40 mmol, 4:1 mix) in 200 mL of toluene was added acetic anhydride (18.8 mL, 200 mmol) in dropwise. The resulting mixture was stirred at room temperature for 3.5 h. The agitation was stopped for 30 min and the precipitate was filtered to provide a product as an off-white solid, 5.45 g (70% yield based on the major isomer), as a single regioisomer. MS *m*/*e* 247 $[M + H]^+$; ^{1}H NMR (400 MHz, DMSO) δ ppm 9.58 (s, 1H), 8.00 (s, 1H), 7.72 (d, 1H), 7.30 (s, 1H), 6.80 (d, 1H), 3.84 (s, 3H), 2.12 (s, 3H), 1.95 (s, 3H).

*Step d. 2-Methoxy-6,7-dimethylimidazo[1,5-a]pyrido[3,2-e]pyrazine (**5**).* To a solution of *N*-(6-methoxy-2-(4-methyl-1*H*-imidazol-1-yl)pyridin-3-yl)acetamide (2.04 g, 8.2 mmol) in 16 mL of $POCl_3$ was added P_2O_5 quickly (minimize the moisture induction). The resulting mixture was refluxed at 110−120 °C for 4 h. $POCl_3$ was evaporated, and the residue was quenched with ice−water very carefully. The mixture was neutralized with saturated Na_2CO_3 solution and extracted with ethyl acetate. The organic layer was dried over magnesium sulfate. Condensation followed by column chromatography using 2−5% MeOH in dichloromethane as eluent provided 2-methoxy-6,7-dimethylimidazo[1,5-*a*]pyrido[3,2-*e*]pyrazine as a yellow powder, 1.12 g (55% yield). MS *m*/*e* 229.0 $[M + H]^+$; ^{1}H NMR (400 MHz, DMSO) δ ppm 8.82 (s, 1H), 8.07 (d, 1H), 6.95 (d, 1H), 3.99 (s, 3H), 2.69 (s, 3H), 2.64 (s, 3H).

*Step e. 9-Bromo-2-methoxy-6,7-dimethylimidazo[1,5-a]pyrido-[3,2-e]pyrazine (**6**).* To a mixture of 2-methoxy-6,7-dimethylimidazo [1,5-*a*]pyrido[3,2-*e*]pyrazine (172 mg, 0.75 mmol) and NBS (200 mg, 1.13 mmol) was added anhydrous CH_3CN (6 mL) under N_2. The resulting solution was stirred in the dark for 24 h. The mixture was concentrated to dryness, and the residue was dissolved in 30 mL of ethyl acetate. The solution was washed twice with brine (2 × 30 mL), saturated Na_2SO_3 solution (20 mL), and brine (20 mL). All aqueous phases were combined and extracted with ethyl acetate (2 × 50 mL). The organic layers were combined and dried over magnesium sulfate. Evaporation under vacuum to dryness provided 9-bromo-2-methoxy-6,7-dimethylimidazo[1,5-*a*]pyrido[3,2-*e*]pyrazine as a light yellow powder (206 mg, 88% yield). MS *m*/*e* 306.9 $[M + H]^+$; ^{1}H NMR (400 MHz, DMSO) δ ppm 8.08 (d, 1H), 7.01 (d, 1H), 4.04 (s, 3H), 2.67 (s, 3H), 2.62 (s, 3H).

*Step f. 2-Methoxy-6,7-dimethyl-9-(4-methylpyridin-3-yl)imidazo[1,5-a]pyrido[3,2-e]pyrazine (**74**).* A mixture of 9-bromo-2-methoxy-6,7-dimethylimidazo[1,5-*a*]pyrido[3,2-*e*]pyrazine (2.0 g, 6.53 mmol), 4-methylpyridine-3-boronic acid (1.79 g, 13.06 mmol), K_2CO_3 (2.70 g, 19.60 mmol), and $Pd(PPh_3)_4$ (150 mg, 0.1306 mmol) in a 250 mL flask was vacuumed and flushed with nitrogen, followed by addition of *p*-dioxane (120 mL) and water (40 mL). The final mixture was stirred at 90 °C for 4 h and then cooled to room temperature. The reaction was quenched with NH_4Cl solution, and the aqueous portion was extracted with ethyl acetate. The combined organic layer was washed with brine and dried over magnesium sulfate. Column chromatography using 50% ethyl acetate in dichloromethane as eluent provided 2-methoxy-6,7-dimethyl-9-(4-methylpyridin-3-yl)imidazo[1,5-*a*]pyrido[3,2- *e*]pyrazine as an off-white powder (1.68 g, 81% yield). MS *m*/*e* 320 $[M + H]^+$; ^{1}H NMR (400 MHz, DMSO) δ ppm 8.55 (s, 1H), 8.50 (m, 1H), 8.10 (d, 1H), 7.40 (m, 1H), 6.85 (d, 1H), 3.10 (s, 3H), 2.75 (s, 3H), 2.70 (s, 3H), 2.05 (s, 3H).

8-Fluoro-6-methoxy-3,4-dimethyl-1-(3-methylpyridin-4-yl)-imidazo[1,5-*a*]quinoxaline (96). *Strep a. 1,5-Difluoro-3-methoxy-2-nitrobenzene (**24**).* To a solution of 3,5-difluoroanisole (30 g, 208 mmol) in 260 mL of dichloromethane was added HNO_3 (>90% fuming, 60 mL) dropwise at 0 °C. The resulting solution was stirred at 0 °C for 3 h and then washed with water. The aqueous phase was extracted with dichloromethane. The combined organics were washed with brine and dried over magnesium sulfate. Evaporation and crystallization in hexane and ethyl acetate provided 1,5-difluoro-3-methoxy-2-nitrobenzene as an off-white powder (28.5 g, 72% yield). MS *m*/*e* 190.1 $[M + H]^+$; ^{1}H NMR (400 MHz, DMSO) δ ppm 7.22 (m, 2H), 3.91 (s, 3H).

*Step b. 2-Bromo-1-(5-fluoro-3-methoxy-2-nitrophenyl)-4-methyl-1H-imidazole (**28**; R_1 = Br, R_6 = OMe, R_8 = F).* A mixture of 1,5-difluoro-3-methoxy-2-nitrobenzene (9 g, 47.6 mmol), 2-bromo-4-methylimidazole (7.7 g, 47.6 mmol), and potassium carbonate (14.5 g, 104.7 mmol) in DMF (240 mL) was stirred at room temperature overnight. The majority of solvent was removed by rotovap, and the residue was diluted with ethyl acetate and washed with water. The aqueous phase was extracted with ethyl acetate, and the combined organics were washed with water and brine and dried over magnesium sulfate. Condensation and purification using 5−10% ethyl acetate in dichloromethane as eluent provided of 2-bromo-1-(5-fluoro-3-methoxy-2-nitrophenyl)-4-methyl-1*H*-imidazole as a yellow solid (4.8 g, 31% yield). MS *m*/*e* 330.0 $[M + H]^+$; ^{1}H NMR (400 MHz, DMSO) δ ppm 7.60 (m, 1H), 7.38 (m, 1H), 7.21 (s, 1H), 3.98 (s, 3H), 2.09 (s, 3H).

*Step c. 4-(1-(5-Fluoro-3-methoxy-2-nitrophenyl)-4-methyl-1H-imidazol-2-yl)-3-methylpyridine (**28a**; R_1 = 3-methylpyridin-4-yl, R_6 = OMe, R_8 = F).* A mixture of 2-bromo-1-(5-fluoro-3-methoxy-2-nitrophenyl)-4-methyl-1*H*-imidazole (2.45 g, 7.4 mmol), 3-picoline-4-boronic acid (1.52 g, 11.1 mmol), K_2CO_3 (3.06 g, 22.2 mmol), and $Pd(PPh_3)_4$ (420 mg, 0.37 mmol) in a 250 mL flask was vacuumed and flushed with nitrogen, followed by the addition of *p*-dioxane (120 mL) and water (40 mL). The final mixture was stirred at 90 °C for 8 h and then cooled to room temperature. The reaction was quenched with NH_4Cl solution, and the aqueous portion was extracted with ethyl acetate. The combined organics were washed with brine and dried over magnesium sulfate. Evaporation and purification by column chromatography using 50%

ethyl acetate in dichloromethane and 4% MeOH in dichloromethane as eluent provided of 4-(1-(5-fluoro-3-methoxy-2-nitrophenyl)-4-methyl-1*H*-imidazol-2-yl)-3-methylpyridine as a yellow solid (1.83 g (72% yield). MS *m/e* 343.1 $[M + H]^+$; ^{1}H NMR (400 MHz, DMSO) δ ppm 8.49 (s, 1H), 8.26 (d, *J* = 5.3 Hz, 1H), 7.44 (m, 1H), 7.23 (m, 1H), 7.21 (s, 1H), 6.94 (d, 1H), 3.89 (s, 3H), 2.31 (s, 3H), 2.18 (s, 3H).

*Step d. N-(4-Fluoro-2-methoxy-6-(4-methyl-2-(3-methylpyridin-4-yl)-1H-imidazol-1-yl)phenyl)acetamide (**31b**; R_1 = 3-methylpyridin-4-yl, R_6 = OMe, R_8 = F, R = COMe).* Into a mixture of 4-(1-(5-fluoro-3-methoxy-2-nitrophenyl)-4-methyl-1*H*-imidazol-2-yl)-3-methylpyridine (1.83 g, 5.3 mmol) and 10% Pd/C (300 mg, 0.265 mmol) was added 30 mL of THF, followed by the addition of MeOH (30 mL) under a nitrogen atmosphere. Ammonium formate (2.0 g, 29.15 mmol) was added to the mixture, and the mixture was stirred at 50 °C for 2 h. The mixture was filtered through a Celite pad, and the solvent was removed under vacuum. The off-white solid residue was taken in toluene (45 mL), and then acetic anhydride (5 mL, 53 mmol) was added. The resulting mixture was stirred at 80 °C for 4 h and cooled to room temperature. The reaction was quenched with sodium bicarbonate solution, and the aqueous portion was extracted 3× with dichloromethane. Evaporation of the solvents and purification by column purification using 3% methanol in dichloromethane as eluent provided *N*-(4-fluoro-2-methoxy-6-(4-methyl-2-(3-methylpyridin-4-yl)-1*H*-imidazol-1-yl)phenyl)acetamide as an off-white solid (1.58 g 84% yield). EI MS *m/e* 355.1 $[M + H]^+$; ^{1}H NMR (400 MHz, DMSO) δ ppm 9.06 (s, 1H), 8.44 (s, 1H), 8.15 (d, *J* = 5.5 Hz, 1H), 7.05 − 6.95 (m, 3H), 6.38 (m, 1H), 3.78 (s, 3H), 2.35 (s, 3H), 2.15 (s, 3H), 1.82 (s, 3H).

*Step e. 8-Fluoro-6-methoxy-3,4-dimethyl-1-(3-methylpyridin-4-yl)-imidazo[1,5-a]quinoxaline (**96**).* Into a mixture of *N*-(4-fluoro-2-methoxy-6-(4-methyl-2-(3-methylpyridin-4-yl)-1*H*-imidazol-1-yl)phenyl)-acetamide (1.58 g, 4.46 mmol) and P_2O_5 (3.16 g, 22.3 mmol) was added $POCl_3$ (60 mL) under nitrogen. The resulting mixture was stirred at 120 °C for 6 h and then cooled to room temperature. The majority of the solvent was removed under vacuum, and the residue was diluted with ethyl acetate. The mixture was transferred slowly into iced 50% NaOH solution. The mixture was stirred for 10 min while maintaining the pH above 7 and then extracted 3× with ethyl acetate. Condensation and column purification using 4% MeOH in dichloromethane as eluent provided 8-fluoro-6-methoxy-3,4-dimethyl-1-(3-methylpyridin-4-yl)imidazo-[1,5-*a*]quinoxaline as an off-white powder (880 mg 60% yield). MS *m/e* 337.1 $[M + H]^+$; ^{1}H NMR (400 MHz, DMSO) δ ppm 8.71 (s, 1H), 8.64 (d, *J* = 5.34 Hz, 1H), 7.52 (d, *J* = 4.89 Hz, 1H), 7.48 (d, 1H), 7.00 (dd, *J* = 11.17, 2.56 Hz, 1H), 6.19 (dd, *J* = 10.47, 2.56 Hz, 1H), 3.91 (s, 3H), 2.75 (s, 3H), 2.69 (s, 3H), 2.00 (s, 3H).

6-Chloro-3,4-dimethyl-1-(3-methylpyridin-4-yl)-8-(trifluoromethyl)imidazo[1,5-*a*]quinoxaline (115). *Step a. 2-Chloro-6-fluoro-4-(trifluoromethyl)aniline (**25a**).* 2-Fluoro-4-(trifluoromethyl)-aniline (5 g, 27.9 mmol) was dissolved in acetonitrile (100 mL). To this was added *N*-chlorosuccinimide (4 g, 30.7 mmol). The mixture was heated to 75 °C for 16 h, then poured into water and extracted with ether. The organic layer was separated and washed with saturated aqueous sodium bicarbonate, then water and brine and dried over $MgSO_4$. The solution was filtered and the solvent removed under reduced pressure to provide 2-chloro-6-fluoro-4-(trifluoromethyl)aniline as a yellow oil (5.2 g). MS *m/e* 212.8 $[M]^+$; ^{1}H NMR (400 MHz, DMSO) δ ppm 7.44 (m, 2H), 6.18 (brs, 2H).

*Step b. 1-Chloro-3-fluoro-2-nitro-5-(trifluoromethyl)benzene (**25b**).* Sodium perborate tetrahydrate (7.3 g, 46.8 mmol) was suspended in glacial acetic acid (30 mL) and heated to 50 °C. Into this mixture was added dropwise a solution of 2-chloro-6-fluoro-4-(trifluoromethyl)aniline (2 g, 9.37 mmol) dissolved in glacial acetic acid (20 mL). The mixture was stirred for 16 h at 50 °C and then poured into water and extracted with ethyl ether. The organic layer was separated and washed with water, aqueous bicarbonate solution, and brine. The organic layer was then dried over $MgSO_4$ and filtered. The solvent was removed under reduced pressure and the crude product purified by flash chromatography on silica gel in hexane to provide 1-chloro-3-fluoro-2-nitro-5-(trifluoromethyl)-benzene as a brown oil (1.17 g). MS *m/e* 242.8 $[M]^+$; ^{1}H NMR (400 MHz, DMSO) δ ppm 8.23−8.29 (m, 2H).

*Step c. 1-(3-Chloro-2-nitro-5-(trifluoromethyl)phenyl)-4-methyl-1H-imidazole (**28**; R_1 = H, R_6 = Cl, R_8 = CF_3).* 1-Chloro-3-fluoro-2-nitro-5-(trifluoromethyl)benzene (1.1 g, 4.5 mmol) and 4-methyl-1*H*-imidazole (0.371 g, 4.5 mmol) were dissolved in DMF (10 mL). To this was added potassium carbonate (1.2 g, 9.0 mmol). The mixture was stirred at room temperature for 16 h and then was poured into water and extracted with ethyl acetate. The organic layer was separated and washed with water, brine and dried over $MgSO_4$. The solution was then filtered and the solvent removed under reduced pressure. The crude was purified by flash chromatography on silica gel in 10:2 hexane/ethyl acetate to provide 1-(3-chloro-2-nitro-5-(trifluoromethyl)phenyl)-4-methyl-1*H*-imidazole as a tan solid (0.74 g). MS *m/e* 306.0 $[M + H]^+$; ^{1}H NMR (400 MHz, DMSO) δ ppm 8.46 (s, 1H), 8.24 (s, 1H), 7.82 (s, 1H), 7.11 (s, 1H), 2.12 (s, 3H).

*Step d. 2-Chloro-6-(4-methyl-1H-imidazol-1-yl)-4-(trifluoromethyl)-aniline (**31a**; R_1 = H, R_6 = Cl, R_8 = CF_3).* 1-(3-Chloro-2-nitro-5-(trifluoromethyl)phenyl)-4-methyl-1*H*-imidazole (0.74 g, 2.4 mmol) was dissolved in a solution of glacial acetic acid and ethanol (10 mL each). Into this mixture was added iron powder (0.81 g, 14.4 mmol). The mixture was heated to 100 °C for 1 h. The mixture was poured into aqueous 1 N sodium hydroxide and extracted with ethyl acetate. The organic layer was separated and then washed with water, brine and dried over $MgSO_4$. The resulting solution was filtered and the solvent removed under reduced pressure to provide 2-chloro-6-(4-methyl-1*H*-imidazol-1-yl)-4-(trifluoromethyl)aniline as an off-white solid (0.68 g). MS *m/e* 274.1 $[M - H]^+$; ^{1}H NMR (400 MHz, DMSO) δ ppm 7.68−7.70 (m, 2H), 7.36 (s, 1H), 7.07 (s, 1H), 5.8 (brs, 2H), 2.15 (s, 3H).

*Step e. N-(2-Chloro-6-(4-methyl-1H-imidazol-1-yl)-4-(trifluoromethyl)-phenyl)acetamide (**31b**; R_1 = H, R_6 = Cl, R_8 = CF_3).* 2-Chloro-6-(4-methyl-1*H*-imidazol-1-yl)-4-(trifluoromethyl)aniline (2 g, 7.26 mmol) was dissolved in a solution of glacial acetic acid (20 mL) and acetic anhydride (10 mL). Into this mixture was added 10 drops of concentrated sulfuric acid. The mixture was stirred at room temperature for 48 h and then poured into ice−water and extracted with ethyl acetate. The organic layer was separated and washed with water, then saturated Na_2CO_3 and then water, brine, dried over $MgSO_4$, and filtered. The solvent was removed under reduced pressure to afford *N*-(2-chloro-6-(4-methyl-1*H*-imidazol-1-yl)-4-(trifluoromethyl)phenyl)acetamide as a tan solid (1.7 g). MS *m/e* 318.1 $[M + H]^+$; ^{1}H NMR (400 MHz, DMSO) δ ppm 9.9 (s, 1H), 8.06 (s, 1H), 7.8 (s, 1H), 7.71 (s, 1H), 7.07 (s, 1H), 2.15 (s, 3H), 1.95 (s, 3H).

*Step f. 6-Chloro-3,4-dimethyl-8-(trifluoromethyl)imidazo[1,5-a]quinoxalines (**32a**; R1 = H, R_6 = Cl, R_8 = CF_3).* *N*-(2-Chloro-6-(4-methyl-1*H*-imidazol-1-yl)-4-(trifluoromethyl)phenyl)acetamide (1.0 g, 3.15 mmol) was suspended in phosphorus oxychloride (10 mL). Into this mixture was added phosphorus pentoxide (3 g, 12.6 mmol). The mixture was heated to 115 °C for 16 h and then poured slowly into ice−water/methanol and was basified with 50% sodium hydroxide. The resulting solution was extracted with ethyl acetate and the organic layer separated and washed with water, brine and dried over $MgSO_4$. The solution was then filtered and the solvent removed under reduced pressure. The crude product was purified by flash chromatography on silica gel in 1:1 hexane/ethyl acetate to provide 6-chloro-3,4-dimethyl-8-(trifluoromethyl)imidazo[1,5-*a*]quinoxaline as a tan solid (0.57 g). MS *m/e* 300.0 $[M + H]^+$; ^{1}H NMR (400 MHz, DMSO) δ ppm 9.28 (s, 1H), 8.69 (s, 1H), 7.95 (s, 1H), 2.78 (s, 3H), 2.66 (s, 3H).

*Step g. 1-Bromo-6-chloro-3,4-dimethyl-8-(trifluoromethyl)imidazo-[1,5-a]quinoxalines (**32b**; R1 = Br, R_6 = Cl, R_8 = CF_3).* 6-Chloro-3,4-dimethyl-8-(trifluoromethyl)imidazo[1,5-*a*]quinoxaline (0.57 g, 1.902

mmol) was suspended in acetonitrile (50 mL). Into this mixture was added *N*-bromosuccinimide (1.3 g, 7.6 mmol). The mixture was protected from light and stirred at room temperature for 48 h and then poured into water and extracted with ethyl acetate. The organic layer was separated and washed with water, then brine and dried over $MgSO_4$ and filtered. The solvent was removed under reduced pressure and the crude product purified by flash chromatography on silica gel in 10:2 hexane/ethyl acetate to provide 1-bromo-6-chloro-3,4-dimethyl-8-(trifluoromethyl)imidazo[1,5-*a*]quinoxaline as a tan solid 90.63 g). MS *m*/*e* 378.0 $[M + H]^+$; ^1H NMR (400 MHz, DMSO) δ ppm 9.28 (s, 1H), 8.11 (s, 1H), 2.79 (s, 3H), 2.68 (s, 3H).

*Step h. 6-Chloro-3,4-dimethyl-1-(3-methylpyridin-4-yl)-8-(trifluoromethyl)imidazo[1,5-a]quinoxaline (**115**).* 1-Bromo-6-chloro-3,4-dimethyl-8-(trifluoromethyl)imidazo[1,5-*a*]quinoxaline (0.1 g, 0.264 mmol) was suspended in a solution of dioxane (4 mL) and water (1 mL). Into this mixture was added potassium carbonate (71 mg, 0.53 mmol), followed by 3-methylpyridin-4-ylboronic acid (0.054 g, 0.396 mmol). Argon was bubbled through the mixture, and tetrakis(triphenylphosphine)palladium(0) (10%mol, 30 mg) was then added. The mixture was sealed and heated to 110 °C for 3 h and then diluted with water and extracted with ethyl acetate. The organic layer was separated, washed with brine, and dried over $MgSO_4$. Evaporation and purification by flash chromatography on silica gel in ethyl acetate provided 6-chloro-3,4-dimethyl-1-(3-methylpyridin-4-yl)-8-(trifluoromethyl)imidazo[1,5-*a*]quinoxaline as a white solid (70 mg, 45% yield). MS *m*/*e* 391.1 $[M + H]^+$; ^1H NMR (400 MHz, DMSO) δ ppm 8.64−8.66 (m, 1H), 7.99 (s, 1H), 7.5−7.6 (m, 2H), 7.11 (s, 1H), 2.9 (s, 3H), 2.78 (s, 3H), 2.11 (s, 3H).

8-(Cyclopropylmethoxy)-6-fluoro-3,4-dimethyl-1-(3-methylpyridin-4-yl)imidazo[1,5-*a*]quinoxaline (121). *Step a. 6-Fluoro-3,4-dimethyl-1-(3-methylpyridin-4-yl)imidazo[1,5-a]quinoxalin-8-ol (**38a**; R_6 = F, R_1 = 3-methylpyridin-4-yl).* Into a solution of 6-fluoro-8-methoxy-3,4-dimethyl-1-(3-methylpyridin-4-yl)imidazo[1,5-*a*]quinoxaline (92 mg, 0.274 mmol) in $ClCH_2CH_2Cl$ (5 mL) was added dropwise boron tribromide (0.129 mL, 1.368 mmol) at 0 °C. The resulting orange suspension was warmed to 80 °C overnight. The reaction was quenched with sodium carbonate solution, and the aqueous portion was extracted 3× with ethyl acetate and dried over $MgSO_4$. Evaporation of the solvents and purification by column chromatography (50−100% ethyl acetate in dichloromethane, followed by 10% methanol in dichloromethane) provided 6-fluoro-3,4-dimethyl-1-(3-methylpyridin-4-yl)imidazo[1,5-*a*]quinoxalin-8-ol as an off-white solid (80 mg, 91% yield). MS *m*/*e* 323.1 $[M + H]^+$; ^1H NMR (400 MHz, DMSO) δ ppm 10.39 (s, 1H), 8.69 (s, 1H), 8.61 (d, *J* = 4.8 Hz, 1H), 7.45 (d, *J* = 5.0 Hz, 1H), 6.72 (dd, *J* = 11.9, 2.5 Hz, 1H), 6.27 (dd, *J* = 2.2, 1.4 Hz, 1H), 2.75 (s, 3H), 2.70 (s, 3H), 2.00 (s, 3H).

*Step b. 8-(Cyclopropylmethoxy)-6-fluoro-3,4-dimethyl-1-(3-methylpyridin-4-yl)imidazo[1,5-a]quinoxaline (**121**).* Into a mixture of 6-fluoro-3,4-dimethyl-1-(3-methylpyridin-4-yl)imidazo[1,5-*a*]quinoxalin-8-ol (60 mg, 0.186 mmol) and cesium carbonate (91 mg, 0.28 mmol) in DMF (2 mL) was added a solution of (bromomethyl)cyclopropane (40 mg, 0.296 mmol) in 1 mL of DMF. The resulting mixture was stirred at 100 °C for 1 h and cooled to room temperature. The mixture was poured into water extracted with ethyl acetate, washed with water, and then dried over magnesium sulfate. Evaporation and purification by column chromatography (50−80% ethyl acetate in dichloromethane) provided 8-(cyclopropylmethoxy)-6-fluoro-3,4-dimethyl-1-(3-methylpyridin-4-yl)imidazo[1,5-*a*]quinoxaline as an off-white solid (13 mg). MS *m*/*e* 377.1 $[M + H]^+$; ^1H NMR (400 MHz, DMSO) δ ppm 8 0.72 (s, 1H), 8.63 (d, *J* = 5.0 Hz, 1H), 7.51 (d, *J* = 4.9 Hz, 1H), 7.00 (m, 1H), 6.22 (m, 1H), 3,38 (m, 2H), 2.78 (s, 3H), 2.72 (s, 3H), 2.02 (s, 3H), 1.02 (m, 1H), 0.56 (m, 2H), 0.18(m, 2H).

Biology. MK-801-Induced Psychosis in Rats. *Animals.* Female Wistar rats (Crl: (WI) BR from Charles River, Germany) weighing 160−180 g were used. They were housed in groups of five under standard conditions on a 12 h light/dark cycle (lights on at 06:00 h) with ad libitum access to water and food (ssniff M/R 15, Spezialdiaten GmbH, Soest/Westfalen, Germany). Experiments were approved by the Committee for Animal Care and Usage of the Federal State of Saxony and carried out in accordance with German animal protection laws.

Experimental Procedure. Elevated locomotor activity and stereotypies induced by the NMDA antagonist MK-801 are generally accepted as relevant readouts in rodents for the positive symptoms of schizophrenia. MK-801 induced stereotypies and hyperactivity in rats after intraperitoneal administration.[20] Locomotor activity of the rats was recorded by the MotiTest apparatus (TSE, Bad Homburg, Germany). The test area consisted of a square arena (45 cm × 45 cm) with protective Plexiglas walls (20 cm high) in which rats can move freely. Horizontal movements were recorded by 32 infrared photocells arranged along the bottom of each wall of the arena. The duration of activity was analyzed using the "ActiMot" computer program (TSE, Bad Homburg, Germany). Stereotyped sniffing was scored by the experimenter every 5 min over a period of 1 h (12 intervals) according to the method described by Andine et al.[20] The scores (0, no stereotyped sniffing; 1, discontinuous sniffing with free interval of >5 s; 2, continuous sniffing) of the 12 intervals were added together for each parameter. On the day of experimentation, rats receive the test compound or vehicle 30 min prior to test onset; 0.1 mg/kg MK-801 was administered intraperitoneally 10 min prior to testing. The rats were placed in the center of the square arena of the MotiTest apparatus 30 min before the start of the experiment to allow them to become accustomed to the environment. The behavior of the rats was then recorded for 1 h.

Statistics. Results were analyzed by one way analysis of variance (ANOVA) when several groups were compared and by *t* test when two groups were compared. Tukey test was used for individual comparisons. $P < 0.05$ was regarded as significant.[21,22]

Conditioned Avoidance Responding in Rats and Mice. Male Sprague−Dawley CD rats (350−450 g) or male CF-1 mice (40−60 g) were individually housed and either maintained (rats) on a food restricted schedule (15 g of standard rodent feed each day after training/testing) or allowed free access to chow (mice). The testing apparatus consists of a stainless steel and Plexiglas test chamber with two 8 in. × 6.5 in. × 8 in. compartments separated by an arched doorway measuring 3.5 in. × 4.5 in. (MED Associates, Burlington, VT). Each of the two floors of the shuttle box comprises a series of stainless steel grid rods and is wired for the presentation of an electric foot shock (0.5 mA). In addition, each side of the chamber is equipped with a stimulus light and tone (Sonalert; Mallory Sonalert, Indianapolis, IN) and multiple infrared beam source/detectors to locate the subjects within the chamber. Subjects that are trained to avoid the foot shock were placed in the experimental chambers for a 4-min habituation period followed by 50 trials presented on a 15 s variable interval schedule (range of 7.5− 22.5 s). Each trial consisted of a 10 s warning tone and stimulus light (conditioned stimulus) followed by a 10 s shock (unconditioned stimulus), presented through the grid floor on the side where the animal was located, in the presence of the tone and light. If an animal crossed through the archway during the initial 10 s of the trial, the tone and light were terminated, and the response was considered an avoidance response. If an animal crossed through the archway after a foot shock was initiated, the tone, light, and shock were terminated, and the response was considered an escape response. If a response was made during an interval, the animal was punished with a 0.5 s shock (0.5 mA). A MED Associates computer with MEDSTATE Notation software controlled the test session and counted the number of trials in which the animal avoided shock, escaped shock, and did not respond. Only animals displaying stable performance (approximately 90% avoidance responding on the training session before test day for rats and 84% avoidance responding for mice) were considered "trained" and included on test day. Training was maintained by at least one nondrug test session each week. Eight animals received

each dose of the test compounds, as well as a vehicle injection (within subject design).

In Vitro Phosphodiesterase Assays. Phosphodiesterases 1B, 2A, 3A, 4A, 5A, 7B, 8A, 9A, 10A, and 11A were generated from full-length human recombinant clones. PDE6 was isolated from bovine retina as described previously.[18] PDE activity was measured with the preferred substrates. For PDE1B, 2A, 3A, 4A, 7B, 8A, 10A, and 11A, cAMP was used, and for PDE5A, 6, and 9A, cGMP was used at a concentration at or below the K_m. PDE1B was activated with calcium/calmodulin and PDE2A with cyclic GMP. Inhibition of PDE activity was measured by scintillation proximity assay at varied compound concentrations and optimized fixed enzyme concentrations for each enzymatic assay. For determination of IC_{50} values, the Hill plot two-parameter model was used.

Screening. *Inhibition of Recombinant PDE10A (Baculovirus/SF21 System).* TheDNA of PDE10A1 (AB 020593, 2340 bp) was synthesized and cloned into vector pCR4.TOPO (Entelechon GmbH, Regensburg, Germany). The gene was then inserted into a baculovirus vector, ligated with the baculovirus DNA, and the enzyme protein was expressed in SF21 cells. To isolate the enzyme, cells were first harvested by centrifugation at 500*g* followed by resuspension in 50 mM Tris-HCl/1 mM EDTA/250 mM sucrosebuffer, pH 7.4. (Sigma, Deisenhofen, Germany; Merck, Darmstadt, Germany) and lysis by sonication (3 × 15 s, Labsonic U, Fa. Braun, Degersheim, Switzerland, level setting "high"). Cytosolic PDE10A was obtained by centrifugation at 48000*g* for 1 h. The supernatant containing the active enzyme was stored at −70 °C. PDE activity was determined by applying a one-step procedure in microtiter plates. The reaction mixture contained 50 mM Tris-HCl/5 mM $MgCl_2$ buffer (pH 7.4. Sigma, Deisenhofen, Germany; Merck, Darmstadt, Germany), 0.1 μM [^{3}H]cAMP (Amersham, Buckinghamshire, U.K.), and the enzyme in a total volume of 100 μL. Nonspecific activity was determined in the absence of enzyme. The reaction was initiated by addition of the substrate solution and carried out at 37 °C for 30 min. Enzymatic activity was stopped by addition of 25 μL Ysi-SPA beads (Amersham-Pharmacia). After 1 h, the mixture was quantified in a liquid scintillation counter for microtiter plates (Microbeta Trilux). Pipetting of the incubation mixture was routinely performed using the Biomek 2000 (Beckman). The optimal amount of enzyme to use per assay was determined for each enzyme preparation batch prior to usage in compound testing. IC_{50} values were determined using the Hill plot, two-parameter model.

Measurement of Striatal Cyclic Nucleotides. Male CF-1 (20−30 g) mice were dosed intraperitoneally with either **96** (0.3 and 3 mg/kg) with 2% Tween 80/0.5% hydroxyethylcellulose in water as vehicle (n = 4 or 8). Control groups received vehicle at equal volumes (10 mL/kg). Mice were sacrificed by focused microwave irradiation (TMW-6402C, 4.0 kW, 1.15 s; Muromachi microwave applicator; Muromachi Kikai Co., Ltd., Tokyo, Japan) 30 min after dosing with indicated. The striata were removed and immediately frozen on dry ice. Samples were stored at −80 °C. For measurement of cyclic nucleotides, frozen striatal tissue was pulverized at dry ice temperature, weighed, and homogenized (Polytron) in 10 volumes of ice-cold 5% trichloroacetic acid in water. The samples were centrifuged at 1500*g* at 4 °C. The supernatants were extracted three times with 5 volumes of water-saturated ether, and the aqueous phase was placed in a 70 °C heat block for 5 min to evaporate the residual ether. Samples were then diluted 2- or 3-fold with ether-extracted 5% trichloroacetic acid in water. Cyclic nucleotide concentrations (pmol/mg tissue) were determined for the diluted samples with cAMP and cGMP enzyme immunoassay kits (Cayman Chemical Company, Ann Arbor, MI). Values are expressed as the fold change of the compound treatment divided by the average of the vehicle-treated samples. Data were graphed as the mean ± SEM using Prism software (GraphPad Software, Inc., San Diego, CA).

Structural Biology: Expression and Purification of the Catalytic Domain of PDE10A. The catalytic domain of PDE10A, spanning residues 339−479, was expressed from *E. coli* at 15 °C for 16 h with a thrombin-cleavable N-terminal His_6 tag. The cells were collected and lysed in 50 mM potassium phosphate (pH 7.5), 300 mM NaCl, 10% glycerol, 15 mM imidazole, 5 mM β-mercaptoethanol, and 2 mM benzamidine. Following clarification, the lysate was bound to nickel-NTA (Qiagen) and eluted with lysis buffer supplemented with 125 mM imidazole. The eluate was diluted 6-fold with 50 mM Tris (pH 8.0), 1 mM DTT, and 10% glycerol and loaded to a HiTrap Q HP column (GE Biosciences). The anion exchange resin was subsequently washed in dilution buffer supplemented with 50 mM NaCl, and PDE10A was eluted over a 20 column volume gradient by competing with dilution buffer containing 1 M NaCl. Appropriate fractions were pooled, and the His tag was removed via thrombin cleavage (Sigma). Following cleavage, thrombin was removed with *p*-aminobenzamide agarose (Sigma) to terminate the reaction. PDE10A was loaded to a Superdex 75 16/60 sizing column (GE Biosciences) pre-equilibrated in 10 mM Hepes (pH 7.5), 150 mM NaCl, and 1 mM DTT. Residual contaminants were removed by briefly batching binding to POROS HS resin and collecting the unbound material containing PDE10A.

Data Deposition. The atomic coordinates of the PDE10A crystal structure for compounds **74** (3SNI),[19] **96** (3SN7), and **115** (3SNL) have been deposited in the Protein Data Bank, Research Collaboratory for Structural Bioinformatics, Rutgers University, New Brunswick, NJ.

Molecular Modeling Calculations. Docking calculations were performed using the Schrodinger software package Maestro (www.schrodinger.com). After the binding site model was validated by redocking of the X-ray ligands, docking of analogues was performed using the GLIDE or CombiGlide with SP (standard precision) scoring. Conformational analysis was performed using Macromodel with the OPLS-AA force fields and a GBSA solvation model implemented in Maestro (www.schrodinger.com).

■ ASSOCIATED CONTENT

Supporting Information. Elemental analysis data, analytical HPLC purity data, and high resolution mass spectrometry characterization data of intermediates and final compounds not listed in the Experimental Section. This material is available free of charge via the Internet at http://pubs.acs.org.

Accession Codes

[†]The atomic coordinates of the PDE10A crystal structure for compounds **74** (3SNI), **96** (3SN7), and **115** (3SNL) have been deposited in the Protein Data Bank, Research Collaboratory for Structural Bioinformatics, Rutgers University, New Brunswick, NJ.

■ AUTHOR INFORMATION

Corresponding Author

*Telephone: 240-529-0866. Facsimile: 301-846-0794. E-mail: malamas.michael@gmail.com.

Present Addresses

[⊥]Lundbeck Research, 215 College Road Paramus, N.J., USA.
[#]Vitae Pharmaceuticals, 502 West Office Center Drive, Fort Washington, PA, USA.
[∞]AstraZeneca, Mereside, Alderley Park SK10 4TG, UK.

■ ABBREVIATIONS USED

PDE10A, phosphodiesterase 10A; cAMP, cyclic adenosine monophosphate; cGMP, cyclic guanine monophosphate; MSN, medium spiny neuron; MK-801, dizocilpine maleate; MED, minimal

effective dose; PDE, cyclic nucleotide phosphodiesterase; LMA, locomotor activity; CAR, conditioned avoidance response; TPSA, topological polar surface area; ADME, absorption, distribution, metabolism, and excretion; SAR, structure−activity relationship

REFERENCES

(1) Manallack, D. T.; Hughes, R. A.; Thompson, P. E. The next generation of phosphodiesterase inhibitors: structural clues to ligand and substrate selectivity of phosphodiesterases. *J. Med. Chem.* **2005**, *48*, 3449–3462.

(2) Odingo, J. O. Inhibitors of PDE4: a review of recent patent literature. *Expert Opin. Ther. Pat.* **2005**, *15*, 773–787.

(3) Rotella, D. Phosphodiesterase 5 inhibitors: current status and potential applications. *Nat. Rev. Drug Discovery* **2002**, *1*, 674–682.

(4) Houslay, M. D.; Schafer, P.; Zhang, K. Y. Keynote review: phosphodiesterase-4 as a therapeutic target. *Drug Discovery Today* **2005**, *10*, 1503–1519.

(5) Bender, A. T.; Beavo, J. A. Cyclic nucleotide phosphodiesterases: molecular regulation to clinical use. *Pharmacol. Rev.* **2006**, *58*, 488–520.

(6) Loughney, K.; Snyder, P. B.; Uher, L.; Rosman, G. J.; Ferguson, K.; Florio, V. A. Isolation and characterization of PDE10A, a novel human 30, 50-cyclic nucleotide phosphodiesterase. *Gene* **1999**, *234*, 109–117.

(7) Fujishige, K.; Kotera, J.; Omori, K. Striatum- and testis-specific phosphodiesterases PDE10A: isolation and characterization of a rat PDE10A. *Eur. J. Biochem.* **1999**, *266*, 1118–1127.

(8) Fujishige, K.; Kotera, J.; Michibata, H.; Yuasa, K.; Takebayashi, S.; Okumura, K.; Omori, K. Cloning and characterization of a novel human phosphodiesterase that hydrolyzes both cAMP and cGMP (PDE10A). *J. Biol. Chem.* **1999**, *274*, 18438–18445.

(9) Soderling, S.; Bayuga, S. J.; Beavo, J. A. Isolation and characterization of a dualsubstrate phosphodiesterase gene family: PDE10A. *Proc. Natl. Acad. Sci. U.S.A.* **1999**, *96*, 7071–7076.

(10) Soderling, S.; Beavo, J. A. Phosphodiestarase inhibitors. *Curr. Opin. Cell Biol.* **1999**, *12*, 174–179.

(11) Zhang, K.; Card, G.; Suzuki, Y.; Artis, R.; Fong, D.; Gillette, S.; Hsieh, D.; Neiman, J.; West, B.; Zhang, C.; Milburn, M.; Kim, S.-H.; Schlessinger, J.; Bollag, G. A glutamine switch mechanism for nucleotide selectivity by phosphodiesterases. *Mol. Cell* **2004**, *15*, 279–286.

(12) Seeger, T. F.; Bartlett, B.; Coskran, T. M.; Culp, J. S.; James, L. C.; Krull, D. L.; Lanfear, J.; Ryan, A. M.; Schmidt, C. J.; Strick, C. A.; Varghese, A. H.; Williams, R. D.; Wylie, P. G.; Menniti, F. S. Immunohistochemical localization of PDE10A in the rat brain. *Brain Res.* **2003**, *985*, 113–126.

(13) Kaiya, H. Second messenger imbalance hypothesis of schizophrenia. *Prostaglandins, Leukotrienes Essent. Fatty Acids* **1992**, *46*, 33–38.

(14) Muly, E. C.; Smith, Y.; Allen, P.; Greengard, P. Signal transduction abnormalities in schizophrenia: the cAMP system. *Psychopharmacol. Bull* **2002**, *36*, 92–105.

(15) Garver, D. L.; Carl Johnson, C.; Kanter, D. R. Schizophrenia and reduced cyclic AMP production: evidence for the role of receptor-linked events. *Life Sci.* **1982**, *31*, 1987–1992.

(16) Hoefgen, N.; Stange, H.; Rudolf Schindler, R.; Lankau, H.-J.; Grunwald, C.; Langen, B.; Egerland, U.; Tremmel, P.; Pangalos, M. N.; Marquis, K. L.; Hage, T.; Harrison, B. L.; Malamas, M. S.; Brandon, N. J.; Kronbach., T. Discovery of imidazo[1,5-*a*]pyrido[3,2-e]pyrazines as a new class of phosphodiesterase 10A inhibitiors. *J. Med. Chem.* **2010**, *53*, 4399–4411.

(17) Miyaura, N.; Suzuki, A. Palladium-catalyzed cross-coupling reactions of organoboron compounds. *Chem. Rev.* **1995**, *95*, 2457–2483.

(18) Grauer, S.; Pulito, V.; Navarra, R.; Kelly, M.; Kelley, C.; Graf, R.; Langen, B.; Logue, S.; Brennan, J.; Jiang, L.; Charych, E.; Egerland, U.; Liu, F.; Marquis, K.; Malamas, M. S.; Hage, T.; Comery, T.; Brandon, N. PDE10A inhibitors show anti-psychotic, pro-cognitive and negative symptom activities suggesting broad-spectrum utility for the treatment of schizophrenia. *J. Pharmacol. Exp. Ther.* **2009**, *331*, 574–590.

(19) Data were collected at Southeast Regional Collaborative Access Team (SER-CAT) 22-ID (or 22-BM) beamline at the Advanced Photon Source, Argonne National Laboratory, IL. Supporting institutions may be found at www.ser-cat.org/members.html. Use of the Advanced Photon Source was supported by the U.S. Department of Energy, Office of Science, Office of Basic Energy Sciences, under Contract No. W-31-109-Eng-38.

(20) Andiné, P.; Widermark, N.; Axelsson, R.; Nyberg, G.; Olofsson, U.; Martensson, E.; Sandberg, M. Characterization of MK-801-induced behavior as a putative rat model of psychosis. *J. Pharmacol. Exp. Ther.* **1999**, *290*, 1393–1408.

(21) *SigmaStat*, version 3.11; Systat Software, Inc.: Chicago, IL, 2004.

(22) *SigmaPlot*, version 9.0; Systat Software, Inc.: Chicago, IL, 2004.

(23) Wallace, A. C.; Laskowski, R. A.; Thornton, J. M. LIGPLOT: a program to generate schematic diagrams of protein−ligand interactions. *Protein Eng.* **1995**, *8*, 127–134.